An efficient numerical PDE approach for pricing foreign exchange interest rate hybrid derivatives☆

Duy Minh Dang[a,*], Christina C. Christara[b], Kenneth R. Jackson[b], Asif Lakhany[c]

[a]David R. Cheriton School of Computer Science, University of Waterloo, Waterloo, ON, N2L 3G1, Canada
[b]Department of Computer Science, University of Toronto, Toronto, ON, M5S 3G4, Canada
[c]Algorithmics Inc., Toronto, ON, M5T 2C6, Canada

Abstract

We discuss efficient pricing methods via a Partial Differential Equation (PDE) approach for long-dated foreign exchange (FX) interest rate hybrids under a three-factor multi-currency pricing model with FX volatility skew. The emphasis of the paper is on Power-Reverse Dual-Currency (PRDC) swaps with popular exotic features, namely knockout and FX Target Redemption (FX-TARN). Challenges in pricing these derivatives via a PDE approach arise from the high-dimensionality of the model PDE, as well as from the complexities in handling the exotic features, especially in the case of the FX-TARN provision, due to its path-dependency. Our proposed PDE pricing framework for FX-TARN PRDC swaps is based on partitioning the pricing problem into several independent pricing sub-problems over each time period of the swap's tenor structure, with possible communication at the end of the time period. Each of these pricing sub-problems can be viewed as equivalent to a knockout PRDC swap with a known time-dependent barrier, and requires a solution of the model PDE, which, in our case, is a time-dependent parabolic PDE in three space dimensions. Finite difference schemes on non-uniform grids are used for the spatial discretization of the model PDE, and the Alternating Direction Implicit (ADI) timestepping methods are employed for its time discretization. Numerical examples illustrating the convergence properties and efficiency of the numerical methods are provided.

Keywords: Power-Reverse Dual-Currency (PRDC) swaps, Target Redemption (TARN), knockout, Partial Differential Equation (PDE), finite differences, non-uniform grids, Alternating Direction Implicit (ADI)

1. Introduction

The cross-currency/foreign exchange (FX) interest rate derivatives market, like the single-currency one, is driven by investors' interest in structured notes and swaps. In general, the investors are primarily interested in a rate of return as high as possible, as well as in an opportunity to express a view, i.e. to bet, on future directions of the spot FX rate and/or the interest rates. On the other hand, the issuers want to have certain protection against excessive movements in these rates.

In the current era of wildly fluctuating exchange rates, cross-currency interest rate derivatives, especially the FX interest rate hybrid derivatives, referred to as hybrids, are of enormous practical importance. In particular, long-dated (maturities of 30 years or more) FX interest rate hybrids, such as Power-Reverse Dual-Currency (PRDC) swaps, are among the most liquid cross-currency interest rate derivatives [38]. For cross-currency interest rate swaps in general, and PRDC swaps in particular, popular exotic features, such as Bermudan cancelable, knockout and Target Redemption (TARN), are often included, since they appeal to both the investors as an additional yield enhancement strategy, and to the issuers as a protection against

☆This research was supported in part by the Natural Sciences and Engineering Research Council (NSERC) of Canada.

*Corresponding author

Email addresses: dm2dang@uwaterloo.ca (Duy Minh Dang), ccc@cs.toronto.edu (Christina C. Christara), krj@cs.toronto.edu (Kenneth R. Jackson), asif.lakhany@algorithmics.com (Asif Lakhany)

excessive movements in the spot FX rate. Although Bermudan cancelability is typically favored by the issuers, as it gives the issuers the right to cancel the underlying swap at any of the dates of the swap's tenor structure, this exotic feature is usually disliked by many investors, since it does not provide an indication as to when the underlying PRDC swap could be pre-maturely terminated [35]. On the other hand, a possibility of early termination of a cross-currency interest rate swap with a knockout or a TARN feature is explicitly linked to the movements of the spot FX rate and/or the interest rates. As a result, these two exotic features do not have the afore-mentioned problem of Bermudan cancelable swaps, and hence, they are usually favored by the investors. More specifically, in the context of PRDC swaps, a knockout feature usually stipulates that the associated underlying PRDC swap pre-maturely terminates on the first date of the swap's tenor structure on which the spot FX rate exceeds a specified level. In a PRDC swap with a TARN feature, the sum of all FX-linked PRDC coupon amounts paid to date is recorded, and the underlying swap is terminated prematurely on the first date of the tenor structure when the accumulated PRDC coupon amount, including the coupon amount scheduled on that date, has reached or exceeded a pre-determined target cap. Hence, this exotic feature is usually referred to as the FX-TARN.

As FX interest rate derivatives, such as PRDC swaps, are exposed to moves in both the spot FX rate and the interest rates in both currencies, multi-factor pricing models having at least three factors, namely the domestic and foreign interest rates and the spot FX rate, must be used for the valuation of such derivatives. A popular choice for pricing PRDC swaps is Monte-Carlo (MC) simulation. However, this approach has several major disadvantages, such as slow convergence for problems in low-dimensions, i.e. fewer than five dimensions, and the limitation that the price is obtained at a single point only in the domain, as opposed to the global character of the Partial Differential Equation (PDE) approach. In addition, MC methods usually suffer from difficulty in computing accurate hedging parameters, such as delta and gamma, especially when dealing with the TARN feature [35]. On the other hand, challenges in pricing these derivatives via a PDE approach arise primarily from the "curse of dimensionality" associated with high-dimensional PDEs, as well as from the complexities in handling the exotic features, especially in the case of the FX-TARN provision, due to its path-dependency. Also, in the context of interest rate swaps, additional complexity arises due to multiple cash flows. As a result, the pricing of such derivatives via the PDE approach is highly challenging. While there are a few papers on the PDE-based pricing of the TARN feature in the literature, such as [7, 35], they are limited to the context of single-currency notes. To the best of our knowledge, efficient PDE-based pricing of FX interest rate swaps, such as PRDC swaps, with knockout and FX-TARN features in a multi-currency context has not been previously studied in the literature. This shortcoming motivated our work.

In this paper, we discuss an efficient numerical PDE approach for pricing FX interest rate swaps with knockout and FX-TARN provisions, with emphasis on the path-dependency of the FX-TARN feature. We adopt the three-factor pricing model with FX volatility skew proposed in [34]. The major contributions of the paper are:

- We present an efficient PDE pricing framework for FX-TARN PRDC swaps. Our approach uses an auxiliary path-dependent state variable to keep track of the accumulated PRDC coupon amount. This allows us to partition the pricing problem of these derivatives into several independent pricing sub-problems over each period of the swap's tenor structure, each of which corresponds to a discretized value of the auxiliary variable, with possible communication at the end of each time period. We show that each of the afore-mentioned pricing sub-problems can be viewed as equivalent to a knockout PRDC swap with a known time-dependent barrier.

- To numerically solve each of the pricing sub-problems, which, in our case, is a time-dependent parabolic

PDE in three space dimensions, we construct and investigate the performance of certain pre-determined non-uniform grids with centered finite differences (FDs) for the discretization of the space variables of the PDE, while utilizing efficient Alternating Direction Implicit (ADI) timestepping techniques for its time discretization.

- We present numerical examples demonstrating the convergence of the numerical methods, as well as their efficiency. We also analyze the profiles of the value function of the knockout and FX-TARN PRDC swaps.

The remainder of this paper is organized as follows. In Section 2, we first describe the dynamics, knockout and FX-TARN provisions, as well as the financial motivation for PRDC swaps. We then introduce a three-factor pricing model and the associated PDE. Numerical methods and pricing algorithms for knockout and FX-TARN PRDC swaps are described in detail in Section 3. Numerical results are presented and discussed in Section 4. Section 5 concludes the paper and outlines possible future work.

2. Power-Reverse Dual-Currency swaps

2.1. Introduction

A "vanilla" PRDC swap is similar to a "vanilla" single-currency fixed-for-floating [1, 4] interest rate swap, in which both parties, namely the issuer and the investor, agree that the issuer pays the investor a stream of so-called PRDC coupon amounts, and in return, receives the investor's domestic LIBOR payments. (Usually, the issuer of a PRDC swap is a bank.) However, in a PRDC swap, the PRDC coupon amounts are linked to the spot FX rate prevailing when the PRDC coupon rate is set. Here, the spot FX rate is defined as the number of units of domestic currency per one unit of foreign currency. Both the PRDC coupon rate and the domestic floating rate are applied on the same domestic currency notional, denoted by N_d. Unless otherwise stated, we investigate PRDC swaps from the perspective of the issuer of the PRDC coupons. From this perspective, the investor's domestic LIBOR payments represent the stream of fund inflows, and hence, are usually referred to as the *funding leg*.

To be more specific, we consider the tenor structure

$$T_0 = 0 < T_1 < \cdots < T_\beta < T_{\beta+1} = T, \quad \nu_\alpha = T_\alpha - T_{\alpha-1}, \quad \alpha = 1, 2, \ldots, \beta + 1, \tag{2.1}$$

where ν_α represents the year fraction between $T_{\alpha-1}$ and T_α using a certain day counting convention, such as the Actual/365 day counting one [4]. Unless otherwise stated, in this paper, the sub-scripts "d" and "f" are used to indicate domestic and foreign, respectively. Let $P_d(t, \overline{T})$ be the prices at time $t \leq \bar{T}$ in domestic currency of the domestic zero-coupon discount bonds with maturity $\overline{T}$. For use later in the paper, define

$$T_{\alpha^+} = T_\alpha + \delta \text{ where } \delta \to 0^+, \quad T_{\alpha^-} = T_\alpha - \delta \text{ where } \delta \to 0^+, \tag{2.2}$$

i.e. T_{α^-} and T_{α^+} are instants of time just before and just after the date T_α, respectively.

Given the tenor structure (2.1), for a "vanilla" PRDC swap, at each time $\{T_\alpha\}_{\alpha=1}^{\beta}$, there is an exchange of a PRDC coupon amount for a domestic LIBOR floating-rate payment. More specifically, the funding leg pays the amount $\nu_\alpha L_d(T_{\alpha-1}, T_\alpha) N_d$ at time T_α for the period $[T_{\alpha-1}, T_\alpha]$. Here, $L_d(T_{\alpha-1}, T_\alpha)$ denotes the domestic LIBOR rate for the period $[T_{\alpha-1}, T_\alpha]$, as observed at time $T_{\alpha-1}$. This rate is simply-compounded and is defined by [1, 4]

$$L_d(T_{\alpha-1}, T_\alpha) = \frac{1 - P_d(T_{\alpha-1}, T_\alpha)}{\nu_\alpha P_d(T_{\alpha-1}, T_\alpha)}. \tag{2.3}$$

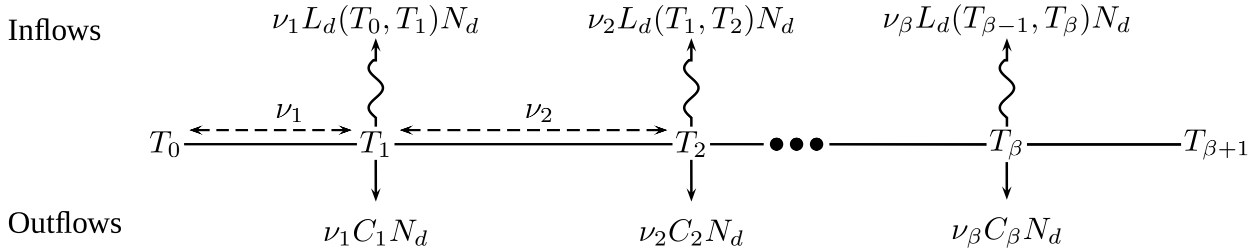

Figure 2.1: Fund flows in a "vanilla" PRDC swap. Inflows and outflows are from the perspective of the PRDC coupon issuer, usually a bank.

Note that $L_d(T_{\alpha-1},T_\alpha)$ is set at time $T_{\alpha-1}$, but the actual floating leg payment for the period $[T_{\alpha-1},T_\alpha]$ does not occur until time T_α.

Throughout the paper, we denote by $s(t)$ the spot FX rate prevailing at time t. The PRDC coupon rate C_α, $\alpha = 1,2,\ldots,\beta$, of the coupon amount $\nu_\alpha C_\alpha N_d$ issued at time T_α for the period $[T_\alpha, T_{\alpha+1}]$, $\alpha = 1,2,\ldots,\beta$, has the structure

$$C_\alpha = \min\left(\max\left(c_f \frac{s(T_\alpha)}{f_\alpha} - c_d, b_l\right), b_c\right), \tag{2.4}$$

where c_d and c_f respectively are domestic and foreign coupon rates; b_l and b_c respectively are the floor and cap of the payoff. The scaling factor f_α is usually set to the forward FX rate $F(0,T_\alpha)$ defined by [1]

$$F(0,T_\alpha) = \frac{P_f(0,T_\alpha)}{P_d(0,T_\alpha)} s(0), \tag{2.5}$$

which follows from no-arbitrage arguments. All parameters c_d, c_f, b_f, and b_c in (2.4) can vary from coupon to coupon, i.e. they may depend on $\{T_\alpha\}_{\alpha=1}^{\beta}$. However, to simplify the notation, we do not indicate the time-dependence of these parameters. A diagram of fund flows in a "vanilla" PRDC swap is presented in Figure 2.1.[1]

In the so-called *standard structure*, which is based on the most commonly used parameter settings, $b_l = 0$ and $b_c = \infty$, and by letting

$$h_\alpha = \frac{c_f}{f_\alpha}, \text{ and } k_\alpha = \frac{c_d}{c_f} f_\alpha, \tag{2.6}$$

the PRDC coupon rate C_α can be viewed as a call option on FX rates, since, in this case, C_α reduces to

$$C_\alpha = h_\alpha \max(s(T_\alpha) - k_\alpha, 0). \tag{2.7}$$

As a result, the PRDC coupon leg in a "vanilla" PRDC swap can be viewed as a portfolio of long-dated options on the spot FX rate, i.e. long-dated FX options.

Usually, there is a settlement in the form of an initial fixed-rate coupon between the issuer and the investor at time T_0 that is not included in the description above. This signed coupon is typically the value at time T_0 of the swap to the issuer, i.e. the value at time T_0 of all net fund flows in the swap, with a positive value of the fixed-rate coupon indicating a fund outflow for the issuer or a fund inflow for the investor, i.e. the issuer pays the investor. Conversely, a negative value of this coupon indicates a fund inflow for the issuer.

[1] Note that in the above setting, the last period $[T_\beta, T_{\beta+1}]$ of the swap's tenor structure is redundant, since there is no exchange of fund flows at time $T_{\beta+1}$. However, to be consistent with [34], we follow Piterbarg's notation.

In (2.7), the *option notional* h_α determines the overall level of the coupon payment, while the strike k_α determines the likelihood of the positiveness of the coupon. It is important to emphasize that, if the strike k_α is low compared to $s(T_\alpha)$, the PRDC coupon has a relatively high chance of paying a positive amount. However, in this case, the option notional h_α is typically chosen to be low also, and hence, the overall level of the PRDC coupon amount paid at time T_α is small. This is a *low-leverage* situation, from the perspective of the investor. On the other hand, if both k_α and h_α are high, then we have a *high-leverage* situation. Note that the leverage level of a PRDC swap is affected by the ratio of c_d and c_f, and not by their absolute values: the absolute values of c_d and c_f only affect the overall coupon amount.

2.2. The model and the associated PDE

In order to model the evolution of the spot FX rate and of the domestic and foreign short rates, we consider the multi-currency model with the FX volatility skew proposed in [34]. We denote by $s(t)$ the spot FX rate, and by $r_i(t), i = d, f$, the domestic and foreign short rates, respectively. Under the domestic risk-neutral measure, the dynamics of $s(t), r_d(t), r_f(t)$ are described by [15]

$$\begin{aligned}
\frac{ds(t)}{s(t)} &= (r_d(t) - r_f(t))dt + \gamma(t, s(t))dW_s(t), \\
dr_d(t) &= (\theta_d(t) - \kappa_d(t)r_d(t))dt + \sigma_d(t)dW_d(t), \\
dr_f(t) &= (\theta_f(t) - \kappa_f(t)r_f(t) - \rho_{fs}(t)\sigma_f(t)\gamma(t, s(t)))dt + \sigma_f(t)dW_f(t),
\end{aligned} \tag{2.8}$$

where $W_d(t), W_f(t)$, and $W_s(t)$ are correlated Brownian motions with

$$dW_d(t)dW_s(t) = \rho_{ds}dt, \quad dW_f(t)dW_s(t) = \rho_{fs}dt, \quad dW_d(t)dW_f(t) = \rho_{df}dt.$$

The short rates follow the mean-reverting Hull-White model [24] with deterministic mean reversion rates and volatility functions, respectively denoted by $\kappa_i(t)$ and $\sigma_i(t)$, for $i = d, f$, while $\theta_i(t)$, $i = d, f$, also deterministic, capture the current term structures. Note that the "quanto" drift adjustment, $-\rho_{fs}(t)\sigma_f(t)\gamma(t, s(t))$, for $dr_f(t)$ comes from changing the measure from the foreign risk-neutral measure to the domestic risk-neutral one [33]. The local volatility function $\gamma(t, s(t))$ for the spot FX rate has the functional form [34]

$$\gamma(t, s(t)) = \xi(t)\Big(\frac{s(t)}{\ell(t)}\Big)^{\varsigma(t)-1}, \tag{2.9}$$

where $\xi(t)$ is the relative volatility function, $\varsigma(t)$ is the time-dependent constant elasticity of variance (CEV) parameter and $\ell(t)$ is a time-dependent scaling constant which is usually set to the forward FX rate $F(0, t)$, for convenience in calibration [34].

Let $u \equiv u(s,r_d,r_f,t)$ denote the domestic value function of a PRDC swap at time t, $T_{\alpha-1} \le t < T_\alpha$, $\alpha = \beta, \ldots, 1$. Given a terminal payoff at maturity time T_α, then on $\mathbb{R}_+ \times \mathbb{R} \times \mathbb{R} \times [T_{\alpha-1}, T_\alpha)$, u satisfies the PDE [15][2]

$$\begin{aligned}
\frac{\partial u}{\partial t} + \mathcal{L}u \equiv \frac{\partial u}{\partial t} &+ \frac{1}{2}\gamma^2(t,s(t))s^2\frac{\partial^2 u}{\partial s^2} + \frac{1}{2}\sigma_d^2(t)\frac{\partial^2 u}{\partial r_d^2} + \frac{1}{2}\sigma_f^2(t)\frac{\partial^2 u}{\partial r_f^2} \\
&+ \rho_{ds}\sigma_d(t)\gamma(t,s(t))s\frac{\partial^2 u}{\partial s\partial r_d} + \rho_{fs}\sigma_f(t)\gamma(t,s(t))s\frac{\partial^2 u}{\partial s\partial r_f} + \rho_{df}\sigma_d(t)\sigma_f(t)\frac{\partial^2 u}{\partial r_d\partial r_f} \\
&+ (r_d - r_f)s\frac{\partial u}{\partial s} + \Big(\theta_d(t) - \kappa_d(t)r_d\Big)\frac{\partial u}{\partial r_d} + \Big(\theta_f(t) - \kappa_f(t)r_f - \rho_{fs}\sigma_f(t)\gamma(t,s(t))\Big)\frac{\partial u}{\partial r_f} - r_d u = 0.
\end{aligned} \tag{2.10}$$

[2] Here, we assume that u is sufficiently smooth on the domain $\mathbb{R}_+ \times \mathbb{R} \times \mathbb{R} \times [T_{\alpha-1}, T_\alpha)$

Since we solve the PDE backward in time, the change of variable $\tau = T_\alpha - t$ is used. Under this change of variable, the PDE (2.10) becomes

$$\frac{\partial u}{\partial \tau} = \mathcal{L}u \tag{2.11}$$

and is solved forward in τ. The pricing of cross-currency interest rate derivatives in general, and PRDC swaps in particular, is defined in an unbounded domain

$$\{(s, r_d, r_f, \tau) | s \geq 0, -\infty < r_d < \infty, -\infty < r_f < \infty, \tau \in [0, T]\}, \tag{2.12}$$

where $T = T_\alpha - T_{\alpha-1}$. Here, $-\infty < r_d < \infty$ and $-\infty < r_f < \infty$, since the Hull-White model can yield any positive or negative value for the interest rate. To solve the PDE (2.11) numerically by FD methods, we truncate the unbounded domain into a finite-sized computational one

$$\{(s, r_d, r_f, \tau) \in [0, s_\infty] \times [-r_{d,\infty}, r_{d,\infty}] \times [-r_{f,\infty}, r_{f,\infty}] \times [0, T]\} \equiv \Omega \times [0, T], \tag{2.13}$$

where s_∞, $r_{d,\infty}$ and $r_{f,\infty}$ are sufficiently large [22, 42].

Since payoffs and fund flows are deal-specific, we defer specifying the terminal conditions until Section 3. The difficulty with choosing boundary conditions is that, for an arbitrary payoff, they are not known. A detailed analysis of the boundary conditions is not the focus of this paper; we leave it as a topic for future research. For this paper, following [16], we impose Dirichlet-type "stopped process" boundary conditions where we stop the processes $s(t), r_f(t), r_d(t)$ when any of the three hits the boundary of the finite-sized computational domain. Thus, the value on the boundary is simply the discounted payoff for the current values of the state variables [16], and is given by

$$u(s, r_d, r_f, \tau) = P_d(\tau, T)u(s, r_d, r_f, T),$$

where

i. either $s = 0$ or $s = s_\infty$,

ii. either $r_d = -r_{d,\infty}$ or $r_d = r_{d,\infty}$, and

iii. either $r_f = -r_{f,\infty}$ or $r_f = r_{f,\infty}$.

Here, $P_d(\tau, T)$ under a Hull-White model can be easily computed (see, for example, [4]). These artificial boundary conditions may induce additional approximation errors in the numerical solutions. However, we can make these errors sufficiently small by choosing suffficiently large values for $s = s_\infty$, $r_{d,\infty}$, and $r_{f,\infty}$. We verify this in numerical tests reported in Section 4.

We conclude this section by noting that the Cox-Ingersoll-Ross (CIR) model [8, 9], which guarantees positive instantaneous short rates, can be used for the domestic and foreign short rates in the pricing model (2.8). The numerical methods developed in this paper are also expected to work well in this case. It would be interesting to compare the effects of various choices for the interest short rate models on the prices of PRDC swaps. We plan to investigate this issue further in the future.

2.3. Exotic variations

Currently, the three most popular exotic features are Bermudan cancelable, knockout and FX-TARN. All three features allow, under different conditions, the pre-mature termination of the underlying PRDC swap after a *no-call* period, usually $[T_0, T_{1^-}]$. The reader is referred to [11, 15] for a detailed discussion of efficient PDE-based numerical methods for "vanilla" and Bermudan cancelable PRDC swaps. Efficient pricing of Bermudan cancelable PRDC swaps using MC simulations in a cross-currency LIBOR market setting can be found in [2]. Below, we describe PRDC swaps with knockout and FX-TARN provisions.

2.3.1. Knockout PRDC swaps

A typical example of a knockout provision is an *up-and-out* FX-linked barrier: the associated underlying PRDC swap pre-maturely terminates on the first date $T_\alpha, \alpha = 1, 2, \ldots, \beta$, of the tenor structure on which the spot FX rate $s(T_\alpha)$ exceeds a specified level. Different variations of the knockout feature may allow the termination of the PRDC swap to occur immediately either before (less common) or after (more common) the occurrence of any exchange of fund flows scheduled on that date. The knockout provisions may allow the barrier to be either constant, i.e. the barrier is the same for all T_α, $\alpha = 1, 2, \ldots, \beta$, or time-dependent (moving), i.e. the barrier changes at each date T_α, $\alpha = 2, \ldots, \beta - 1$. In the context of PRDC swaps, a moving barrier is usually a step-down one [39], i.e. the barrier reduces by a pre-determined amount at each date T_α, $\alpha = 2, \ldots, \beta - 1$, of the swap's tenor structure (in forward time). In this paper, we consider only knockout PRDC swaps with a constant upper barrier, hereinafter denoted by b. The pricing of knockout PRDC swaps with a (time-dependent) step-down barrier is presented in the context of FX-TARN PRDC swaps, and is based on straightforward modifications of the pricing of the constant barrier case. In particular, as shown in Section 3.6, over each time period of the swap's tenor structure, the pricing of FX-TARN PRDC swaps via a PDE approach can be divided into multiple pricing sub-problems, each of which corresponds to a knockout PRDC swap with a pre-determined step-down barrier.

Below we explain how the knockout provision is modelled. Let $\hat{u}_\alpha(t)$ be the value at time t of a knockout PRDC swap that has $\{T_{\alpha+1}, \ldots, T_\beta\}$ as knockout opportunities, i.e. the swap is still alive at time T_α. In particular, the quantity $\hat{u}_0(T_0)$ is the value of the knockout PRDC swap that we are interested in at time T_0. If the PRDC swap has not been knocked out up to and including time T_α, the value $\hat{u}_{\alpha-1}(T_{\alpha^+})$ is equal to $\hat{u}_\alpha(T_{\alpha^+})$. On the other hand, if $s(T_\alpha) > b$, i.e. the swap knocks out at time T_α, the quantity $\hat{u}_{\alpha-1}(T_{\alpha^+})$ is zero. That is, the condition for the possible early termination of a knockout PRDC swap at each of the dates $\{T_\alpha\}_{\alpha=1}^{\beta}$ is enforced by

$$\hat{u}_{\alpha-1}(T_{\alpha^+}) = \begin{cases} 0 & \text{if } s(T_\alpha) > b, \\ \hat{u}_\alpha(T_{\alpha^+}) & \text{otherwise}. \end{cases} \tag{2.14}$$

In Subsection 3.5, we discuss how to enforce (2.14) on a computational grid within the backward pricing algorithm for knockout PRDC swaps.

2.3.2. FX-TARN PRDC swaps

In a FX-TARN PRDC swap, the PRDC coupon amount, $\nu_\alpha C_\alpha N_d$, $\alpha = 1, 2, \ldots$, is recorded. The PRDC swap is pre-maturely terminated on the first date $T_{\alpha_\ell} \in \{T_\alpha\}_{\alpha=1}^{\beta}$ when the accumulated PRDC coupon amount, including the coupon amount scheduled on that date, reaches or exceeds a pre-determined target cap, hereinafter denoted by a_c. That is, the associated underlying PRDC swap terminates immediately on the first date $T_{\alpha_\ell} \in \{T_\alpha\}_{\alpha=1}^{\beta}$ when

$$\sum_{\alpha=1}^{\alpha_\ell} \nu_\alpha C_\alpha N_d \geq a_c. \tag{2.15}$$

Depending on how the PRDC coupon amount scheduled on the early termination date T_{α_ℓ} is handled, there are three versions of FX-TARN PRDC swaps.

1. The last PRDC coupon amount at the early termination date T_{α_ℓ} is set to $a_c - \sum_{\alpha=1}^{\alpha_\ell - 1} \nu_\alpha C_\alpha N_d$ so that the accumulated PRDC coupon amount on termination at T_{α_ℓ} is *exactly* a_c.
2. The PRDC coupon amount paid at each date T_α of the tenor structure is capped at a_c. Note that this allows the accumulated PRDC coupon amount to exceed a_c at the early termination date T_{α_ℓ}, but the accumulated PRDC coupon cannot exceed $2a_c$.

3. This coupon is paid in full.

To illustrate the difference between the three versions of the FX-TARN, consider the following example. For simplicity, let the notional $N_d = 1$. Assume that $a_c = 10\%$, and that $\sum_{\alpha=1}^{\alpha_\ell - 1} \nu_\alpha C_\alpha = 8\%$, i.e. the swap is still "alive" at time $T_{(\alpha_\ell - 1)^+}$. Furthermore, assume that the PRDC coupon amount scheduled on the date T_{α_ℓ}, as calculated by formula (2.4), is 16%. If the first version of the FX-TARN applies, instead of a 16% coupon, the issuer pays only a $2\% (= 10\% - 8\%)$ coupon. However, if the second version of the FX-TARN applies, the issuer pays a 10% ($= \min(a_c, 16\%)$) coupon, whereas, if the third version of the FX-TARN applies, the issuer pays the entire 16% coupon. In all three cases, the underlying PRDC swap pre-maturely terminates at time T_{α_ℓ}. Note that, during the life of the swap, in the first version of the FX-TARN, exactly 10% ($= 8\% + 2\% = a_c$) of the notional is paid. However, in the second and third versions of the FX-TARN, 18% ($= 8\% + 10\%$) and 24% ($= 8\% + 16\%$), respectively, of the notional are paid, both of which are greater than a_c. As noted above, the second version of the FX-TARN ensures a cap of $2a_c$ on the accumulated PRDC coupon amount, while the third version provides no cap at all.

In practice, the first version of the FX-TARN is more popular among issuers than the other two, due to its stronger protection against the unfavorable movements in the spot FX rate. In this paper, we consider mainly the first version of the FX-TARN feature, due to its popularity. In Subsection 3.6.4, we discuss extensions of the numerical methods developed in this paper to price the second and third versions of the FX-TARN PRDC swaps.

Below, we describe the modelling and updating rules of the FX-TARN feature of PRDC swaps. We observe a similarity between the TARN feature of a PRDC swap and the knockout feature of an Asian barrier option which is governed by the average asset value [43]. Following [43], our PDE pricing approach for FX-TARN PRDC swaps is based on an auxiliary path-dependent state variable, hereinafter denoted by $a(t)$, $0 \leq a(t) < a_c$, which represents the accumulated PRDC coupon amount. This variable stays constant between dates of the swap's tenor structure and is updated on each date of the tenor structure to reflect the PRDC coupon amount known on that date. It can be used to determine the pre-mature termination of the underlying swap on that date.

The value of a FX-TARN PRDC swap depends on four stochastic state variables, namely $s(t)$, $r_d(t)$, $r_f(t)$ and the path-dependent variable $a(t)$. We denote by $u \equiv u(s, r_d, r_f, t; a)$ the domestic value function of a FX-TARN PRDC swap.

For presentation purposes, we further adopt the following notation: $a_{\alpha^+} \equiv a(T_{\alpha^+}), a_{\alpha^-} \equiv a(T_{\alpha^-})$. It is important to note that, since $a(t)$ changes only on the dates $\{T_\alpha\}_{\alpha=1}^{\beta}$, the pricing PDE does not depend on $a(t)$. More specifically, apart from dates $\{T_\alpha\}_{\alpha=1}^{\beta}$, for any fixed value of a, the function u satisfies the model-dependent PDE (2.10). Moreover, on each of the dates $\{T_\alpha\}_{\alpha=1}^{\beta}$, assuming that $a_{\alpha^-} < a_c$, i.e. the swap is still alive at time T_{α^-}, the quantity a changes according to the updating rule

$$a_{\alpha^+} = a_{\alpha^-} + \min(a_c - a_{\alpha^-}, \nu_\alpha C_\alpha N_d) \equiv a_{(\alpha-1)^+} + \min(a_c - a_{(\alpha-1)^+}, \nu_\alpha C_\alpha N_d), \tag{2.16}$$

where we have used $a_{\alpha^-} = a_{(\alpha-1)^+}$, since, as noted above, $a(t)$ changes only on the dates $\{T_\alpha\}_{\alpha=1}^{\beta}$. The quantity $\min(a_c - a_{\alpha^-}, \nu_\alpha C_\alpha N_d)$ in (2.16) is the actual PRDC coupon amount paid at T_α, taking into account the fact that the target cap for the total coupon amount must be exactly a_c. (See version 1 of a FX-TARN PRDC swap described on page 7.) When $a_{\alpha^+} = a_c$, the swap terminates. By no-arbitrage arguments, across each date $\{T_\alpha\}_{\alpha=1}^{\beta}$, u must satisfy the updating rule

$$u(s, r_d, r_f, T_{\alpha^+}; a_{\alpha^+}) = u(s, r_d, r_f, T_{\alpha^-}; a_{\alpha^-}) + \nu_\alpha L_d(T_{\alpha-1}, T_\alpha) N_d - \min(a_c - a_{\alpha^-}, \nu_\alpha C_\alpha N_d). \tag{2.17}$$

REMARK 2.1. We observe from (2.16) that, at each date T_α, $\alpha = \beta, \ldots, 1$, assuming that $a_{\alpha^-} < a_c$, there is a value of the spot FX rate, hereinafter denoted by b_α, for which $a_{\alpha^+} = a_c$, i.e. the underlying swap terminates on the date T_α, if $s(T_\alpha) \geq b_\alpha$. The value b_α is in fact path-dependent (as expected), and is known at time $T_{(\alpha-1)^+}$, when $a_{\alpha^-} = a_{(\alpha-1)^+}$ is available, and can be obtained by solving for $s(T_\alpha)$ from

$$\nu_\alpha C_\alpha N_d = a_c - a_{\alpha^-} \iff \nu_\alpha h_\alpha \max(s(T_\alpha) - k_\alpha, 0) N_d = a_c - a_{\alpha^-},$$

where we have used the definition (2.7) for C_α. That is,

$$b_\alpha = \frac{a_c - a_{\alpha^-}}{\nu_\alpha h_\alpha N_d} + k_\alpha = \frac{a_c - a_{\alpha^-}}{\nu_\alpha c_f N_d} f_\alpha + \frac{c_d}{c_f} f_\alpha > k_\alpha, \tag{2.18}$$

where we have substituted $h_\alpha = \frac{c_f}{f_\alpha}$ and $k_\alpha = \frac{c_d}{c_f} f_\alpha$ as defined in (2.6). As noted in Subsection 2.4, f_α decreases steeply as T_α increases, and thus, so does the strike k_α. Furthermore, a_α is an increasing function of T_α, i.e. $a_{\alpha^-} > a_{(\alpha-1)^-}$. Hence, from (2.18), we can see that b_α decreases as T_α increases. As a result, a FX-TARN PRDC swap is essentially a knockout PRDC swap with a path-dependent step-down upper barrier.

2.4. *Financial motivation for PRDC swaps*

Below, we briefly outline a few important points associated with the financial motivation for PRDC swaps with exotic features that are essential to understand this paper. A more complete discussion of the dynamics and investment strategies associated with PRDC swaps can be found in the literature, e.g. in [29, 38, 39].

The origin of PRDC swaps as well as the interest in these structured products are closely related to the search for yield enhancements by domestic currency investors when the interest rate for the domestic currency is low relative to the interest rate for the foreign currency. More specifically, if the interest rate for the domestic currency (e.g. Japanese Yen (JPY)) is low relative to the interest rate for the foreign currency (e.g. United States Dollar (USD) or Australian Dollar (AUD)), the forward FX rate curve $F(0, t), t > 0$, computed by the no-arbitrage formula (2.5), decreases steeply as t increases, predicting a significant strengthening of the domestic currency. However, historical data suggests that the future spot FX rate will remain near its current level. This is reflected in the coupon rate formula (2.4): the investor receives a positive coupon at time T_α if $s(T_\alpha)$ is sufficiently large compared to $f_\alpha \equiv F(0, T_\alpha)$. Thus, the investor can be viewed as betting that the domestic currency is not going to strengthen as much as predicted by the forward FX rate curve. Essentially, the investor's strategy in a PRDC swap is similar to the so-called "carry trade", a very popular trading strategy for currency investors in FX markets [31].

The exotic features, such as those described earlier, provide protection, from the perspective of the issuer, against excessive movements in the spot FX rate via a possible early termination of the swap. However, from the perspective of the investor, these exotic features can be viewed as an additional yield-enhancing mechanism which provides a higher rate of return in the form of a higher fixed-rate coupon paid by the issuer to the investor during the *no-call* period, usually at time T_0. More specifically, in a PRDC swap with an exotic feature, such as knockout or FX-TARN, the issuer can be viewed as "buying" from the investor a right to protect themselves against unfavorable movements in the spot FX rate. As a result, a positive value (to the issuer) from such a position is generated and contributes to a higher positive initial fixed-rate coupon at time T_0, i.e. a higher fund inflow for the investor at time T_0. Therein lies the main attraction of the exotic features to the investor: this initial fixed-rate coupon paid by the issuer to the investor is usually much higher than the rate of return that the investor can obtain anywhere else. In addition, the investor benefits even more from an exotic feature if the swap terminates quickly. For example, if the underlying PRDC swap is terminated at time T_1, the investor essentially pays a low domestic LIBOR payment $\nu_1 L_d(T_0, T_1) N_d$ and receives a very high initial fixed-rate coupon on top of the PRDC coupon amount $\nu_1 C_1 N_d$ (or possibly a reduced coupon as described in Subsection 2.3.2.)

3. Numerical methods

In this section, we discuss the discertization of the model PDE (2.11) and the pricing algorithms for knockout and FX-TARN PRDC swaps.

3.1. Discretization of the model PDE

Let the number of sub-intervals be $n+1$, $p+1$, $q+1$, and l in the s-, r_d-, r_f-, and τ-directions, respectively. As described below in Subsections 3.2 and 3.3, we use a fixed, but not necessarily uniform, spatial grid together with dynamically chosen timestep sizes. These spatial and temporal stepsizes are denoted by $\Delta s_i = s_i - s_{i-1}$, $\Delta r_{d,j} = r_{d,j} - r_{d,j-1}$, $\Delta r_{f,k} = r_{f,k} - r_{f,k-1}$, and $\Delta \tau_m = \tau_m - \tau_{m-1}$, where $i = 1, \ldots, n+1$, $j = 1, \ldots, p+1$, $k = 1, \ldots, q+1$, and $m = 1, \ldots, l$, respectively. Let the gridpoint values of a FD approximation to the solution u be denoted by $u^m_{i,j,k} \approx u(s_i, r_{d,j}, r_{f,k}, \tau_m)$.

For the discretization of the space variables in the differential operator $\mathcal{L}$ of (2.11), we employ FD *central* schemes in the interior of the rectangular domain Ω. For example, at the reference point $(s_i, r_{d,j}, r_{f,k}, \tau_m)$, the first and second derivatives with respect to the spot FX rate s, i.e. $\dfrac{\partial u}{\partial s}$ and $\dfrac{\partial^2 u}{\partial s^2}$, are approximated by

$$\frac{\partial u}{\partial s} \approx \alpha_{i,-1} u^m_{i-1,j,k} + \alpha_{i,0} u^m_{i,j,k} + \alpha_{i,1} u^m_{i+1,j,k}, \tag{3.1}$$

and

$$\frac{\partial^2 u}{\partial s^2} \approx \beta_{i,-1} u^m_{i-1,j,k} + \beta_{i,0} u^m_{i,j,k} + \beta_{i,1} u^m_{i+1,j,k}, \tag{3.2}$$

respectively, where

$$\begin{aligned} &\alpha_{i,-1} = -\frac{\Delta s_{i+1}}{\Delta s_i(\Delta s_i + \Delta s_{i+1})}, \quad \alpha_{i,0} = \frac{(\Delta s_{i+1} - \Delta s_i)}{\Delta s_i \Delta s_{i+1}}, \quad \alpha_{i,+1} = \frac{\Delta s_i}{\Delta s_{i+1}(\Delta s_i + \Delta s_{i+1})}, \\ &\beta_{i,-1} = \frac{2}{\Delta s_i(\Delta s_i + \Delta s_{i+1})}, \beta_{i,0} = -\frac{2}{\Delta s_i \Delta s_{i+1}}, \beta_{i,+1} = \frac{2}{\Delta s_{i+1}(\Delta s_i + \Delta s_{i+1})}. \end{aligned} \tag{3.3}$$

Denote by $\bar{\alpha}_{j,\tilde{j}}$ and $\bar{\beta}_{j,\tilde{j}}$, where $\tilde{j} = \{-1, 0, 1\}$, the coefficients analogous to $\alpha_{i,\tilde{i}}$ and $\beta_{i,\tilde{i}}$ in (3.1) and (3.2), respectively, but relevant to the r_d-direction, and defined in a similar way as in (3.3). Similarly, for the r_f-direction, the corresponding coefficients are denoted by $\bar{\bar{\alpha}}_{k,\tilde{k}}$ and $\bar{\bar{\beta}}_{k,\tilde{k}}$. The cross-derivatives in (2.11) are approximated by a nine-point (3×3) FD stencil.[3] For instance, at the reference point $(s_i, r_{d,j}, r_{f,k}, \tau_m)$, for the discretization of the cross-derivative $\dfrac{\partial^2 u}{\partial s \partial r_d}$, we use the FD scheme

$$\frac{\partial^2 u}{\partial s \partial r_d} \approx \sum_{\tilde{i},\tilde{j}=-1}^{1} \alpha_{i,\tilde{i}} \bar{\alpha}_{j,\tilde{j}} u^m_{i+\tilde{i},j+\tilde{j},k}, \tag{3.4}$$

which can be viewed as obtained by successively applying the FD scheme (3.1) in the s- and r_d-directions. Similar FD schemes can be derived for the cross-derivatives $\dfrac{\partial^2 u}{\partial s \partial r_f}$ and $\dfrac{\partial^2 u}{\partial r_d \partial r_f}$. Details about our choice of the non-uniform spatial grids are given in Subsection 3.3.

[3] On uniform grids, the nine-point FD stencil reduces to a four-point one.

Let $\mathbf{u}^m$ denote the vector of values of the unknown prices at time τ_m on the mesh Ω that approximates the exact solution $u^m = u(s, r_d, r_f, \tau_m)$. We denote by $\mathbf{A}^m$ the matrix of size $npq \times npq$ arising from the FD discretization of the differential operator $\mathcal{L}$ at τ_m.

For the time discretization of the PDE (2.11), we employ the ADI timestepping technique based on the Hundsdorfer and Verwer (HV) splitting approach [25, 26], henceforth referred to as the *HV scheme*. We note that problems containing cross-derivatives were not discussed in [25, 26]. In fact, the schemes based on the HV splitting approach for problems containing cross-derivatives were first proposed and analyzed in [27] (for the case of two-dimensional convection-diffusion parabolic PDEs), and in [28] (for the case of multi-dimensional diffusion parabolic PDEs).

Following the HV approach, we decompose the matrix $\mathbf{A}^m$ into four sub-matrices: $\mathbf{A}^m = \mathbf{A}_0^m + \mathbf{A}_1^m + \mathbf{A}_2^m + \mathbf{A}_3^m$. The matrix $\mathbf{A}_0^m$ is the part of $\mathbf{A}^m$ that comes from the FD discretization of the cross-derivative terms in (2.11), while the matrices $\mathbf{A}_1^m$, $\mathbf{A}_2^m$ and $\mathbf{A}_3^m$ are the three parts of $\mathbf{A}^m$ that correspond to the spatial derivatives in the s-, r_d-, and r_f-directions, respectively. The term $r_d u$ in $\mathcal{L}u$ is distributed evenly over $\mathbf{A}_1^m$, $\mathbf{A}_2^m$ and $\mathbf{A}_3^m$. Starting from $\mathbf{u}^{m-1}$, the HV scheme generates an approximation $\mathbf{u}^m$ to the exact solution u^m, $m = 1, \ldots, l$, by[4]

$$
\begin{cases}
\mathbf{v}_0 = \mathbf{u}^{m-1} + \Delta\tau_m(\mathbf{A}^{m-1}\mathbf{u}^{m-1} + \mathbf{g}^{m-1}), & \text{(3.5a)}\\
(\mathbf{I} - \theta\Delta\tau_m\mathbf{A}_i^m)\mathbf{v}_i = \mathbf{v}_{i-1} - \theta\Delta\tau_m\mathbf{A}_i^{m-1}\mathbf{u}^{m-1} + \theta\Delta\tau_m(\mathbf{g}_i^m - \mathbf{g}_i^{m-1}), \quad i = 1, 2, 3, & \text{(3.5b)}\\
\widetilde{\mathbf{v}}_0 = \mathbf{v}_0 + \dfrac{1}{2}\Delta\tau_m(\mathbf{A}^m\mathbf{v}_3 - \mathbf{A}^{m-1}\mathbf{u}^{m-1}) + \dfrac{1}{2}\Delta\tau_m(\mathbf{g}^m - \mathbf{g}^{m-1}), & \text{(3.5c)}\\
(\mathbf{I} - \theta\Delta\tau_m\mathbf{A}_i^m)\widetilde{\mathbf{v}}_i = \widetilde{\mathbf{v}}_{i-1} - \theta\Delta\tau_m\mathbf{A}_i^m\mathbf{v}_3, \quad i = 1, 2, 3, & \text{(3.5d)}\\
\mathbf{u}^m = \widetilde{\mathbf{v}}_3. & \text{(3.5e)}
\end{cases}
$$

In (3.5), the vector $\mathbf{g}^m$ is given by $\mathbf{g}^m = \sum_{i=0}^{3}\mathbf{g}_i^m$, where $\mathbf{g}_i^m$ are obtained from the boundary conditions corresponding to the respective spatial derivative terms.

The free parameter θ in (3.5) is directly related to the stability and accuracy of the HV ADI scheme. We note that results on the stability of the various ADI schemes applied to three-dimensional pure diffusion parabolic PDEs with cross-derivatives have been derived in [28]. More specifically, it has been shown in [28] that, in this case, the HV scheme is stable whenever $\theta \geq \frac{3}{2}(2 - \sqrt{3})(\approx 0.402)$. However, sufficient conditions on θ for stability of the HV scheme applied to three-dimensional convection-diffusion parabolic PDEs with cross-derivatives, such as the one in this paper, have not been yet established in the literature. For the two-dimensional convection-diffusion parabolic PDEs, the conjecture in [27] is that the HV scheme is unconditionally stable for all $\theta \geq \frac{1}{2} + \frac{1}{6}\sqrt{3}(\approx 0.7887)$. This value of θ was successfully used in [22] for the three-dimensional PDE arising from the hybrid Heston-Hull-White model [23, 24]. We also note that smaller values of θ often give better accuracy.

Since the payoff functions are discontinuous at each date of the tenor structure, in order to take advantage of the damping property of the HV scheme when $\theta = 1$ [25], we first apply the HV scheme with $\theta = 1$ for the first few (usually two) initial timesteps, and then switch to $\theta = \frac{1}{2} + \frac{1}{6}\sqrt{3}$ for the remaining timesteps. We refer to this timestepping technique as *HV smoothing*. We emphasize that choosing the parameter $\theta = 1$ gives a "partially" implicit timestepping method only, not a fully implicit one. Hence, HV smoothing is not the same as Rannacher smoothing [37], which initially uses a few (usually two or three) steps of fully implicit timestepping before switching to another timestepping method, such as Crank-Nicolson [10].

[4] This is the scheme (1.4) in [28] with $\mu = \frac{1}{2}$.

The HV splitting scheme treats the cross-derivative part ($\mathbf{A}_0^m$) in a fully-explicit way, while the $\mathbf{A}_i^m$ parts, $i = 1, 2, 3$, are treated implicitly. Relations (3.5a) and (3.5b) can be viewed as an explicit Euler predictor step followed by three implicit, but unidirectional, corrector steps aiming to stabilize the predictor step. Several well-known ADI methods, such as the Douglas and Rachford method [17], are special instances of these two steps. The purpose of the additional stages (3.5c) and (3.5d) that compute $\widetilde{\mathbf{v}}_i, i = 0, \ldots, 3$, is to restore second-order convergence for the general case with cross-derivatives, while retaining the unconditional stability of the scheme. The FD discretization for the spatial variables described in (3.1) and (3.2) implies that, if the gridpoints are ordered appropriately, the matrices $\mathbf{A}_1^m$, $\mathbf{A}_2^m$ and $\mathbf{A}_3^m$ are block-diagonal with tridiagonal blocks. (We assume a different ordering for each of $\mathbf{A}_1^m$, $\mathbf{A}_2^m$ and $\mathbf{A}_3^m$.) As a result, the number of floating-point operations per time step is directly proportional to npq, which yields a big reduction in computational cost compared to the application of a direct method, such as the LU factorization, to solve the problem arising from a FD time discretization, such as Crank-Nicolson.[5]

3.2. Timestep size selector

We use a simple, but effective, timestep size selector presented in [19] that was shown to work well in the context of pricing options (e.g. see [6] and [19]). The idea underlying this scheme is to predict a suitable timestep size for the next timestep, using only information from the current and previous timesteps. We extend this timestep size selector for use with ADI timestepping methods applied to pricing PRDC swaps.

According to the formula in [19], given the current stepsize $\Delta\tau_m$, $m \geq 1$, the new stepsize $\Delta\tau_{m+1}$ is given by

$$\begin{cases} \Delta\tau_{m+1} &= \left(\min_{1 \leq \iota \leq npq} \left[\dfrac{\texttt{dnorm}}{\frac{|\mathbf{u}_\iota^m - \mathbf{u}_\iota^{m-1}|}{\max(N, |\mathbf{u}_\iota^m|, |\mathbf{u}_\iota^{m-1}|)}} \right] \right) \Delta\tau_m, \\ \Delta\tau_{m+1} &= \min\left\{ \Delta\tau_{m+1}, T - \tau_m \right\}. \end{cases} \tag{3.6}$$

Here, `dnorm` is a user-defined target relative change, and the scale N is chosen so that the method does not take an excessively small stepsize where the value of the option is small. Normally, for option values in dollars, $N = 1$ is used. We use $N = 1$ for PRDC swap pricing too. In all our experiments, we used $\Delta\tau_1 = 10^{-2}$ and `dnorm` $= 0.3$ on the coarsest grids. The value of `dnorm` is reduced by two at each refinement, while $\Delta\tau_1$ is reduced by four.

3.3. Algorithms for constructing non-uniform partitions

In this subsection, we briefly describe algorithms that produce non-uniform, but fixed, partitions of an interval with denser points in the regions of practical importance. The algorithms make use of a function that maps uniform grids to non-uniform ones. The mapping function, based on the $\sinh$ function, considered in this paper was first suggested in [40]. Variations of it appear frequently in the literature (e.g. [6, 32]).

Our aim is to construct a non-uniform partition of $[l, u]$ with e sub-intervals, that are more concentrated around the point $c \in [l, u]$. In addition, we also want to have some control over the density of the partition points on the left and the right sides of the point c. To this end, we associate the parameters d_l and d_u with the densities of points in the sub-regions $[l, c]$ and $[c, u]$, respectively. More specifically, the quantities $\frac{1}{d_l}$ and $\frac{1}{d_u}$ represent the density of points in the respective regions, with a larger density giving rise to a partition that is denser toward the point c in the associated sub-region. We also choose $i \in \{0, 1, \ldots, e\}$ and set the i-th gridpoint in the non-uniform partition to be equal to c. Thus, there are i sub-intervals in the sub-region $[l, c]$

[5] When Crank-Nicolson timestepping method is employed, iterative methods with preconditioning techniques are usually utilized to solve the resulting matrix problem. See [15] for an example of this approach.

and $(e-i)$ sub-intervals in the sub-region $[c, u]$. Hence, the numbers of gridpoints in the sub-regions $[l, c]$ and $[c, u]$ can be controlled by choosing an appropriate value for i. For example, by choosing $i = \texttt{ceil}(0.3e)$, where `ceil` denotes the ceiling function, approximately 30% of the total number of sub-intervals will be in the sub-region $[l, c]$, and the rest will be in the sub-region $[c, u]$. Non-uniform partitions for $[l, u]$ are defined as images of uniform partitions, and can be constructed as described in Algorithm 3.1

Algorithm 3.1 Algorithm for constructing a non-uniform partition of an interval with one concentration point.

PartitionOne$(l, u, c, e, i, d_l, d_u)$

1: compute $g_l = \sinh^{-1}\left(\frac{l-c}{d_l}\right)$ and $g_u = \sinh^{-1}\left(\frac{u-c}{d_u}\right)$;
2: compute $z_0 = l; z_j = c + d_l \sinh(g_l(1-k_j))$, where $k_j = \frac{j}{i}$, $j = 1, \ldots, i$; set $P_l = \{z_j\}_{j=0}^{i}$;
3: compute $z_j = c + d_u \sinh(g_u k_j)$, where $k_j = \frac{j}{e-i}$, $j = 1, \ldots, (e-i)$; set $P_u = \{z_j\}_{j=1}^{e-i}$;
4: return $P \equiv P_l \cup P_u$.

REMARK 3.1. The procedure described in Algorithm 3.1 can be easily tailored to generate non-uniform partitions that are dense towards either of the two endpoints, l or u. For example, choosing $c = u$ and $i = e$ in the above procedure gives rise to a non-uniform partition that is more concentrated towards the upper endpoint u. We use this type of non-uniform partition later in this paper for the auxiliary state variable employed in pricing FX-TARN PRDC swaps. This is discussed in Remark 3.6.

Algorithm 3.1 can be used to construct a sub-partition for a non-uniform partition with more than one concentration points. We use it in Algorithm 3.2 to generate a non-uniform partition having N sub-intervals for the region $[L, U]$ with concentration points c_j, $j = 1, \ldots, v$, satisfying $L \leq c_1 < c_2 < \ldots < c_v \leq U$. Here, e_j is the number of sub-intervals for the j-th sub-region containing c_j, $j = 1, \ldots, v$, with $\sum_{j=1}^{v} e_j = N$; i_j is the local index of the gridpoint in the j-th sub-region that is equal to c_j; d_l^j and d_u^j are the upper and lower density parameters, respectively, associated with the j-th sub-region containing c_j.

Algorithm 3.2 Algorithm for constructing a non-uniform partition of an interval with multiple concentration points.

PartitionMulti$(L, U, \{c_j\}_{j=1}^{v}, \{e_j\}_{j=1}^{v}, \{i_j\}_{j=1}^{v}, \{d_l^j\}_{j=1}^{v}, \{d_u^j\}_{j=1}^{v})$

1: $P_1 \leftarrow PartitionOne\left(L, \frac{c_1+c_2}{2}, c_1, e_1, i_1, d_l^1, d_u^1\right)$;
2: $P_j \leftarrow PartitionOne(\frac{c_{j-1}+c_j}{2}, \frac{c_j+c_{j+1}}{2}, c_j, e_j, i_j, d_l^j, d_u^j)$, $j = 2, \ldots, v-1$;
3: $P_v \leftarrow PartitionOne(\frac{c_{v-1}+c_v}{2}, U, c_v, e_v, i_v, d_l^v, d_u^v)$;
4: return $P \equiv \cup_{j=1}^{v} P_j$.

We conclude this section by noting that the non-uniform grids constructed using Algorithm 3.2 may possibly yield "jumps" in the grid stepsizes at the points near where the two sub-regions are pasted, resulting in possibly non-smooth grid partitions. In this case, the truncation error of the FD scheme 3.2 for the second spatial derivatives is only first-order approximation. However, since this problem may occur only at just a few points and the jumps are relatively small, it may not impair the overall second-order convergence of the methods. As illustrated in Section 4 on the numerical results, second-order convergence of the numerical methods are preserved.

3.4. Non-uniform spatial partitions

Non-uniform partitions in the r_d- and r_f-directions are relatively straight-forward to construct. More specifically, we can apply Algorithm 3.1 to build non-uniform partitions with the concentration points being the initial domestic and foreign interest short rates $r_d(0)$ and $r_f(0)$, and use the same partitions for all time periods of the swap's tenor structure.

With respect to the partitions in the spot FX direction, since (i) the PRDC coupon leg in a PRDC swap can be viewed as a portfolio of options on the spot FX rate, i.e. FX options, and (ii) the possibility of early termination is also directly linked to the spot FX rate, properly constructed non-uniform grids for the spot FX rate variable s are crucial for the efficiency of the PDE-based pricing methods. In the rest of this subsection, we describe how to construct effective non-uniform partitions of the spot FX rate s for knockout PRDC swaps with constant barrier. Due to the path-dependency of the FX-TARN feature, the construction of effective non-uniform partitions of the spot FX rate in the case of FX-TARN PRDC swaps requires further discussions, and is given in a later subsection, Subsection 3.6.2.

For a knockout PRDC swap with a constant barrier, there are two regions of practical importance in the s-direction. The first one is around the strike k_α, which is the initial kink point in the payoff function (2.7) at each date T_α, $\alpha = \beta, \ldots, 1$. It is important to note that each k_α is known in advance and is fully determined by the domestic and foreign interest rate curves and the initial spot FX rate. The second important region is around the (constant) upper barrier b, due to the discontinuities of the terminal condition at each date T_α, $\alpha = \beta, \ldots, 1$, of the swap's tenor structure. (This is noted in Remark 3.2.) As a result, in this case, it would be desirable to have non-uniform partitions that are concentrated around k_α and b. Algorithm 3.2 can be used to construct non-uniform partitions for the spot FX rate. For the rest of the paper, for knockout PRDC swaps, we denote by

$$\Delta_\alpha \equiv \{s_{\alpha,0} \equiv 0 < s_{\alpha,1} < \cdots < s_{\alpha,n} < s_{\alpha,n+1} \equiv s_\infty\}$$

the non-uniform partition generated by Algorithm 3.2 for the variable s used for the solution of the model PDE over the time period $[T_{(\alpha-1)^+}, T_{\alpha^-}]$, $\alpha = \beta, \ldots, 1$. Two examples of such non-uniform partitions are given in Figure 3.1.

In Figure 3.2, we give an example of the spot FX rate curve, the strikes k_α, $\alpha = \beta, \ldots, 1$, and other relevant data. In this example, the tenor structure is $T_\alpha = 1, \ldots, 29$ (years), The domestic and foreign interest rate curves are given by $P_d(0,t) = \exp(-0.02 \times t)$ and $P_f(0,t) = \exp(-0.05 \times t)$. The initial spot FX rate is set to $s(0) = 105.0$, domestic and foreign coupons are $c_d = 8.1\%, c_f = 9.0\%$, and the fixed upper barrier is $b = 131.25$. These data are used for experiments with the high-leverage case reported in Subsection 4.1. We plot the forward FX rate curve $F(0,t)$ as a function of time t (marked by stars). Note that $F(0,t)$ is defined by $F(0,t) = \dfrac{P_f(0,t)}{P_d(0,t)} s(0)$, (see (2.5)). Note that, due to the interest rate differential between the two currencies, with r_d being considerably smaller than r_f, the quantity $P_f(0,t)/P_d(0,t)$ decreases substantially as t increases. Thus, as illustrated in Figure 3.2, the forward FX rate curve is steeply downward sloping as t increases. We also plot the strikes k_α, $\alpha = \beta, \ldots, 1$, at selected dates of the tenor structure (marked by black dots). Note that, since $k_\alpha = \dfrac{c_d}{c_f} f_\alpha \equiv \dfrac{c_d}{c_f} F(0, T_\alpha)$, according to (2.6), and $\dfrac{c_d}{c_f}$ is fixed, the strikes k_α also decrease as T_α increases. Other relevant data are the initial spot FX rate $s(0) = 105.0$ (marked by a white dot), and the barrier $b = 131.25$ (marked by a plus).

As shown in Figure 3.2, when we proceed backward in time, the strikes k_α move closer to the barrier b from the left, because the forward FX rate curve is downward sloping. Thus, although the non-uniform partitions Δ_α are fixed within each time period $[T_{(\alpha-1)^+}, T_{\alpha^-}]$ of the swap's tenor structure, they should be reconstructed when we proceed to the next time period to capture the new initial kink point $k_{\alpha-1}$. In our approach, at the end of each time period $[T_{(\alpha-1)^+}, T_{\alpha^-}]$, $\alpha = \beta, \ldots, 2$, interpolation along the s-direction of the PDE solution values corresponding to Δ_α must be employed to find the PDE solution values corresponding to $\Delta_{\alpha-1}$. These values then become part of the terminal condition for the solution of the PDE over the next time period $[T_{(\alpha-2)^+}, T_{(\alpha-1)^-}]$. In our numerical experiments, linear interpolation is used.

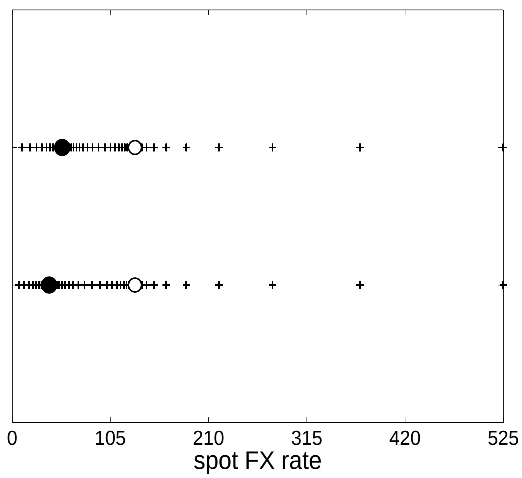

Figure 3.1: Two examples of non-uniform partitions in the s-direction generated by Algorithm 3.2. The concentration points, $s = 39.5$ (bottom) and $s = 53.5$ (top), marked by black dots, play the role of k_α, while $s = 131.25$, marked by a white dot, plays the role of the constant barrier, b.

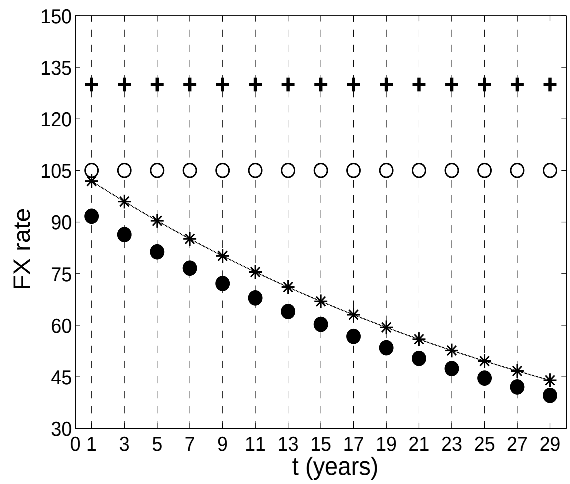

Figure 3.2: An example of the forward FX rate curve (marked by stars), and the strikes k_α (marked by black dots) at selected dates of the tenor structure $T_\alpha = 1, \ldots, 29$ (years). Other relevant data are: $s(0) = 105.0$ (marked by a white dot), $b = 131.25$ (marked by a plus). The data used for the computation are given for the high-leverage case in Subsection 4.1.

3.5. Pricing algorithm for knockout PRDC swaps

Recall that $\hat{u}_\alpha(t)$ denotes the value at time t of a knockout PRDC swap that has $\{T_{\alpha+1}, \ldots, T_\beta\}$ as knockout opportunities. We denote by $\hat{u}_\alpha(s_{\alpha,i}, r_{d,j}, r_{f,k}, t)$ an approximation to $\hat{u}_\alpha(t)$ at the gridpoint $(s_{\alpha,i}, r_{d,j}, r_{f,k})$, $\alpha = \beta, \ldots, 1$, $i = 1, \ldots, n$, $j = 1, \ldots, p$, and $k = 1, \ldots, q$. (Note that the quantity $\hat{u}_0(T_0) \equiv \hat{u}_0(0)$ corresponding to $(s(0), r_d(0), r_f(0))$ is an approximation to the value of the knockout PRDC swap at time T_0 that we are interested in, and can be obtained from $\hat{u}_0(s_{1,i}, r_{d,j}, r_{f,k}, 0)$. See Remark 3.4 for details.) For each T_α, $\alpha = \beta, \ldots, 1$, we assume that the quantities $\hat{u}_\alpha(s_{\alpha,i}, r_{d,j}, r_{f,k}, T_{\alpha^+})$ have been computed at the previous time period of the tenor structure, i.e. these are available at T_{α^+}. On a computational grid, the condition (2.14) for the possible early termination of a knockout PRDC swap is enforced by

$$\hat{u}_{\alpha-1}(s_{\alpha,i}, r_{d,j}, r_{f,k}, T_{\alpha^+}) = \begin{cases} 0 & \text{if } s_{\alpha,i} > b, \\ \hat{u}_\alpha(s_{\alpha,i}, r_{d,j}, r_{f,k}, T_{\alpha^+}) & \text{otherwise}. \end{cases}$$

We now consider the backward pricing algorithm for knockout PRDC swaps from time T_{α^-} to $T_{(\alpha-1)^+}$. One may attempt to start the backward algorithm at time T_{α^-} with the payoff

$$\hat{u}^{(1)}_{\alpha-1}(s_{\alpha,i}, r_{d,j}, r_{f,k}, T_{\alpha^-}) \equiv \hat{u}_{\alpha-1}(s_{\alpha,i}, r_{d,j}, r_{f,k}, T_{\alpha^+}) + \nu_\alpha L_d(T_{\alpha-1}, T_\alpha) N_d - \nu_\alpha C_\alpha N_d, \tag{3.7}$$

where $\nu_\alpha L_d(T_{\alpha-1}, T_\alpha) N_d$ and $\nu_\alpha C_\alpha N_d$ are the funding payment and PRDC coupon amount scheduled at time T_α, respectively. Unfortunately, the above payoff is path-dependent, since the LIBOR rate $L_d(T_{\alpha-1}, T_\alpha)$ is determined at time $T_{\alpha-1}$, but the LIBOR payment takes place at time T_α. To overcome this difficulty, over each period of the swap's tenor structure, we consider the pricing of the funding leg and the PRDC coupon leg separately. The value at time $T_{(\alpha-1)^+}$ of the funding payment scheduled on T_α is simply given by (e.g. see [12])

$$(1 - P_d(T_{\alpha-1}, T_\alpha)) N_d. \tag{3.8}$$

On the other hand, the value at time $T_{(\alpha-1)^+}$ of the PRDC coupon $\nu_\alpha N_d C_\alpha$ is computed by solving the PDE (2.10). To this end, let $\hat{u}^{(2)}_{\alpha-1}(s_{\alpha,i}, r_{d,j}, r_{f,k}, T_{(\alpha-1)^+})$ be the value obtained by solving the PDE (2.10) backward in time from time T_{α^-} to time $T_{(\alpha-1)^+}$ with terminal condition

$$\hat{u}^{(1)}_{\alpha-1}(s_{\alpha,i}, r_{d,j}, r_{f,k}, T_{\alpha^-}) \equiv \hat{u}_{\alpha-1}(s_{\alpha,i}, r_{d,j}, r_{f,k}, T_{\alpha^+}) - \nu_\alpha C_\alpha N_d.$$

We then apply interpolation to $\hat{u}^{(2)}_{\alpha-1}(s_{\alpha,i}, r_{d,j}, r_{f,k}, T_{(\alpha-1)^+})$ along the s-direction, to obtain $\hat{u}^{(3)}_{\alpha-1}(s_{\alpha-1,i}, r_{d,j}, r_{f,k}, T_{(\alpha-1)^+})$. The approximate value of the knockout PRDC swap at time $T_{(\alpha-1)^+}$ on $\Delta_{(\alpha-1)}$ is then given by

$$\hat{u}_{\alpha-1}(s_{\alpha-1,i}, r_{d,j}, r_{f,k}, T_{(\alpha-1)^+}) \equiv \hat{u}^{(3)}_{\alpha-1}(s_{\alpha-1,i}, r_{d,j}, r_{f,k}, T_{(\alpha-1)^+}) + (1 - P_d(T_{\alpha-1}, T_\alpha)) N_d.$$

A backward pricing algorithm for knockout PRDC swaps is presented in Algorithm 3.3.

It should be clear from the discussion earlier that the quantities $\nu_\alpha C_\alpha N_d$ and $(1 - P_d(T_{\alpha-1}, T_\alpha)) N_d$ depend on s, and, on a computational grid, they are computed using discretized values of s. To avoid introducing more notation, throughout the paper, we omit showing the dependence of these quantities on the gridpoint indices.

REMARK 3.2. It is important to note that, due to (3.9), the payoff (3.10) resembles that of a digital option. It is well-known that discontinuities in a digital payoff function can result in a reduction of the observed order of convergence of a numerical scheme [36]. In the context of option pricing, to restore the expected order of convergence, a remedy is to have the strike price positioned midway between the gridpoints [36, 40], an approach referred to as the *grid shifting technique*. We adopt this technique in our numerical method: the grids are chosen so that the fixed upper barrier b lies midway between the gridpoints in the spot FX rate, i.e. the s-direction. It is not necessary to have b as a midpoint of the grid in the r_d- and/or r_f-directions, since the digital condition of the payoff function (3.9) depends only on the spot FX rate $s(t)$. Although other techniques for smoothing the discontinuities in the initial data, such as averaging and projection methods [36], can be used, we adopted the grid shifting technique for our numerical experiments due to its simplicity and effectiveness. In addition, it is worth pointing out that, since discontinuities in the payoff functions may be introduced at each of the times $\{T_\alpha\}_{\alpha=1}^{\beta}$, in our numerical experiments, we apply the HV smoothing technique for each of the dates $\{T_\alpha\}_{\alpha=1}^{\beta}$ of the tenor structure when knockouts are possible. This is similar to the techniques discussed in [41] in the context of discrete barrier options. Our numerical results presented in Section 4 show that this technique provides good damping and works well for PRDC swaps with a knockout provision.

Algorithm 3.3 Backward algorithm for computing knockout PRDC swaps.

construct Δ_β by Algorithm 3.2, and set $\hat{u}_\beta(\cdot,\cdot,\cdot,T_{\beta^+}) = 0$;
for $\alpha = \beta, \ldots, 1$ **do**
  set
$$\hat{u}_{\alpha-1}(s_{\alpha,i}, r_{d,j}, r_{f,k}, T_{\alpha^+}) = \begin{cases} 0 & \text{if} \quad s_{\alpha,i} > b, \\ \hat{u}_\alpha(s_{\alpha,i}, r_{d,j}, r_{f,k}, T_{\alpha^+}) & \text{otherwise}; \end{cases} \tag{3.9}$$
  set
$$\hat{u}^{(1)}_{\alpha-1}(s_{\alpha,i}, r_{d,j}, r_{f,k}, T_{\alpha^-}) = \hat{u}_{\alpha-1}(s_{\alpha,i}, r_{d,j}, r_{f,k}, T_{\alpha^+}) - \nu_\alpha N_d C_\alpha; \tag{3.10}$$
  solve the PDE (2.10) with the terminal condition (3.10) backward in time from T_{α^-} to $T_{(\alpha-1)^+}$ using the ADI scheme (3.5) for each time τ_m, $m = 1, \ldots, l$, with the timestep size $\Delta\tau_m$ selected by (3.6), to obtain $\hat{u}^{(2)}_{\alpha-1}(s_{\alpha,i}, r_{d,j}, r_{f,k}, T_{(\alpha-1)^+})$;
  if $\alpha \geq 2$ **then**
    construct $\Delta_{\alpha-1}$ by Algorithm 3.2;
    apply interpolation to $\hat{u}^{(2)}_{\alpha-1}(s_{\alpha,i}, r_{d,j}, r_{f,k}, T_{(\alpha-1)^+})$ to obtain $\hat{u}^{(3)}_{\alpha-1}(s_{\alpha-1,i}, r_{d,j}, r_{f,k}, T_{(\alpha-1)^+})$;
    set $\hat{u}_{\alpha-1}(s_{\alpha-1,i}, r_{d,j}, r_{f,k}, T_{(\alpha-1)^+}) = \hat{u}^{(3)}_{\alpha-1}(s_{\alpha-1,i}, r_{d,j}, r_{f,k}, T_{(\alpha-1)^+}) + (1 - P_d(T_{\alpha-1}, T_\alpha))N_d$;
  else
    set $\hat{u}_{\alpha-1}(s_{\alpha,i}, r_{d,j}, r_{f,k}, T_{(\alpha-1)^+}) = \hat{u}^{(2)}_{\alpha-1}(s_{\alpha,i}, r_{d,j}, r_{f,k}, T_{(\alpha-1)^+}) + (1 - P_d(T_{\alpha-1}, T_\alpha))N_d$;
  end if
end for
set $\hat{u}_0(\cdot,\cdot,\cdot,T_0) = \hat{u}_0(\cdot,\cdot,\cdot,T_{0^+})$;

REMARK 3.3. The upper barrier b may not be a midpoint between two adjacent gridpoints in the partition Δ_α. To adjust the partitions Δ_α so that the upper barrier b is a midpoint, we proceed as follows. We first construct the partition Δ_α with n sub-intervals instead of $n+1$ sub-intervals using Algorithm 3.2. This partition has $b = s_{\alpha,\bar{i}}$ for some $\bar{i} \in \{1, \ldots, n\}$. We then (i) slightly relocate the gridpoint corresponding to the barrier and (ii) add one extra gridpoint to the area around the barrier as follows:

set $\Delta s_{\alpha,\bar{i}} = \min\{s_{\alpha,\bar{i}} - s_{\alpha,\bar{i}-1}, s_{\alpha,\bar{i}+1} - s_{\alpha,\bar{i}}\}$;
set $s_{\alpha,\bar{i}} \leftarrow s_{\alpha,\bar{i}} - \frac{\Delta s_{\alpha,\bar{i}}}{3}$;
add a gridpoint via $s_{\alpha,\bar{i}+1} \leftarrow s_{\alpha,\bar{i}} + \frac{2\Delta s_{\alpha,\bar{i}}}{3}$;

The barrier is now a midpoint of the two gridpoints $s_{\alpha,\bar{i}}$ (i) and $s_{\alpha,\bar{i}+1}$ (ii).

REMARK 3.4. It is also important to point out that both $r_d(0)$ and $r_f(0)$ are gridpoints in the respective spatial partitions, i.e. $r_d(0) = r_{d,\hat{j}}$ and $r_f(0) = r_{f,\hat{k}}$ for some $\hat{j} \in \{1, \ldots, p\}$ and $\hat{k} \in \{1, \ldots, q\}$. However, $s(0)$ is not guaranteed to be a gridpoint of Δ_1. As a result, to compute an approximate value to $\hat{u}_0(0)$ corresponding to $(s(0), r_d(0), r_f(0)) \equiv (s(0), r_{d,\hat{j}}, r_{f,\hat{k}})$, which is the quantity we are interested in, interpolation along the s-direction using the values $\hat{u}_0(s_{1,i}, r_{d,\hat{j}}, r_{f,\hat{k}}, 0)$, $i = 0, \ldots, n+1$, may be needed. To avoid this possible interpolation, we adjust the partition Δ_1 by adjusting the closest to $s(0)$ gridpoint to be $s(0)$. That is, $s(0) = s_{1,\hat{i}}$ for some $\hat{i} \in \{1, \ldots, n\}$. Hence, an approximate value to $\hat{u}_0(0)$ corresponding to $(s(0), r_d(0), r_f(0))$ is simply given by $\hat{u}_0(s_{1,\hat{i}}, r_{d,\hat{j}}, r_{f,\hat{k}}, 0)$.

3.6. *Pricing algorithm for FX-TARN PRDC swaps*

3.6.1. *Key observation and a general pricing framework*

Generally speaking, in pricing an interest rate swap via a PDE approach, the purpose of the backward procedure from the last date of exchange of fund flows (e.g. T_β in our case) to the date $T_{(\alpha-1)^+}$, $\alpha = \beta, \ldots 1$, is to compute the value at time $T_{(\alpha-1)^+}$ of all the fund flows scheduled on or after T_α in the swap's tenor structure. If a FX-TARN PRDC swap is pre-maturely terminated by the time $T_{(\alpha-1)^+}$, there are no further fund flows scheduled on or after T_α, and, hence, the swap's value is zero. This observation suggests that, over each period $[T_{(\alpha-1)^+}, T_{\alpha^-}]$ of the swap's tenor structure, the backward procedure which computes the solution backward in time from T_{α^-} to $T_{(\alpha-1)^+}$ needs to be invoked only if the swap is still alive at time $T_{(\alpha-1)^+}$, i.e. if $a_{(\alpha-1)^+}$ satisfies $0 \le a_{(\alpha-1)^+} < a_c$. Since we progress backward in time and the variable $a(t)$ is path-dependent, we do not know the exact value of $a_{(\alpha-1)^+}$. However, since $0 \le a_{(\alpha-1)^+} < a_c$, we can discretize the variable a, as we do for other spatial variables. This key observation leads to the following general PDE pricing framework for a FX-TARN PRDC swap:

- (i) across each date $\{T_\alpha\}_{\alpha=\beta}^{1}$ and for each discretized value of the variable a, apply the updating rules (2.16) and (2.17) on the swap values to
  - (a) take into account the fund flows scheduled on that date;
  - (b) reflect changes in the accumulated PRDC coupon amount, and the possibility of early termination;
  - (c) obtain terminal conditions for the solution of the PDE from time T_{α^-} to $T_{(\alpha-1)^+}$ (see Step (ii) below);
- (ii) over each period $[T_{(\alpha-1)^+}, T_{\alpha^-}]$, $\alpha = \beta, \ldots, 1$, of the swap's tenor structure, for each discretized value of the variable a, solve the model PDE (2.10) backward in time from T_{α^-} to $T_{(\alpha-1)^+}$, with the corresponding terminal condition obtained in Step (i.c).

For the rest of the paper, we adopt the following notation. Partition the interval $[0, a_c]$ into $w+1$ sub-intervals having gridpoints

$$0 = a_0 < a_1 < \ldots < a_w < a_{w+1} = a_c. \tag{3.11}$$

Note that, for all periods of the swap's tenor structure, we have the fixed, not necessarily uniform, set of gridpoints (3.11) in the a-direction. (See Remark 3.6 for our choice of non-uniform partitions for the variable a.) Below, we first discuss the construction of non-uniform partitions for the s variable, then describe in detail a PDE-based pricing algorithm for FX-TARN PRDC swaps.

3.6.2. *Non-uniform partitions for the spot FX rate*

In light of Remark 2.1, for each fixed value a_y, $y = 0, \ldots, w$, and at each date T_α, $\alpha = \beta, \ldots, 1$, there is a value of the spot FX rate, hereinafter denoted by b_α^y, for which the underlying swap terminates on the date T_α, if $s(T_\alpha) \ge b_\alpha^y$. Following (2.18), since $a_y, y = 0, \ldots, w$, are fixed for all time periods, the values b_α^y, $y = 0, \ldots, w$, $\alpha = \beta, \ldots, 1$, are known in advance and can be pre-computed via

$$b_\alpha^y = \frac{a_c - a_y}{\nu_\alpha c_f N_d} f_\alpha + \frac{c_d}{c_f} f_\alpha > k_\alpha. \tag{3.12}$$

As a result, each pricing sub-problem, corresponding to a fixed value a_y, $y = 0, \ldots, w$, can be viewed as a knockout PRDC swap with a pre-determined step-down upper barrier b_α^y. (Note that for a fixed α, all sub-problems have the same k_α, but different b_α^y.) Thus, for each a_y, $y = 0, \ldots, w$, and at each T_α, $\alpha = \beta, \ldots, 1$, it is desirable to construct a non-uniform partition for the s variable that is refined in the regions around the strike k_α and the barrier b_α^y. Similar to knockout PRDC swaps with a constant barrier, Algorithm 3.2 can be employed to generate such non-uniform partitions. For the rest of the paper, for FX-TARN PRDC swaps, we denote by

$$\Delta_\alpha^y \equiv \{s_{\alpha,0}^y \equiv 0 < s_{\alpha,1}^y < \ldots < s_{\alpha,n}^y < s_{\alpha,n+1}^y \equiv s_\infty\}$$

the non-uniform partition for the spatial variable s used for the solution of the PDE corresponding to a_y over the time period $[T_{(\alpha-1)^+}, T_{\alpha^-}]$.

REMARK 3.5. From (3.12), for a fixed α, we observe that, if a_y, $y = 0, \ldots, w$, is relatively close to a_c, b_α^y can be relatively close to k_α. In such cases, instead of applying Algorithm 3.2, we can construct a non-uniform partition with only one concentration point centered around the strike k_α using Algorithm 3.1. We can then apply the adjustment mentioned in Remark 3.3, so that the barrier b_α^y falls at a midpoint. In our experiments reported in Section 4 for FX-TARN PRDC swaps, we applied this procedure to construct non-uniform partitions for the s variable whenever $b_\alpha^y - k_\alpha \leq$ `small-range`. In our experiments, the constant `small-range` is selected to be 15 by trial-and-error.

3.6.3. PDE-based pricing algorithm

Let $u_\alpha(t; a)$ represent the value at time t of a FX-TARN PRDC swap that has

(i) $\{T_{\alpha+1}, \ldots, T_\beta\}$ as pre-mature termination opportunities, i.e. the swap is still alive at time T_α; and

(ii) the total accumulated PRDC coupon amount, including the coupon amount scheduled on T_α, is equal to $a < a_c$.

In particular, the quantity $u_0(T_0; 0)$ is the value of the FX-TARN PRDC swap we are interested in at time T_0. If a FX-TARN PRDC swap has not been pre-maturely terminated by time T_α, i.e. $a_{\alpha^+} < a_c$, the value $u_{\alpha-1}(T_{\alpha^+}; a_{(\alpha-1)^+})$ is given by

$$u_{\alpha-1}(T_{\alpha^+}; a_{(\alpha-1)^+}) = u_\alpha(T_{\alpha^+}; a_{\alpha^+}) \equiv u_\alpha(T_{\alpha^+}; a_{(\alpha-1)^+} + \min(a_c - a_{(\alpha-1)^+}, \nu_\alpha C_\alpha N_d)), \tag{3.13}$$

according to the updating rule (2.16). On the other hand, if the swap is terminated at time T_α, we then have $u_{\alpha-1}(T_{\alpha^+}; a_{(\alpha-1)^+}) = 0$. That is, the condition for a possible early termination of a FX-TARN PRDC swap at each of the times $\{T_\alpha\}_{\alpha=1}^\beta$ is enforced by

$$u_{\alpha-1}(T_{\alpha^+}; a_{(\alpha-1)^+}) = \begin{cases} 0 & \text{if } a_{\alpha^+} \geq a_c, \\ u_\alpha(T_{\alpha^+}; a_{\alpha^+}) & \text{otherwise,} \end{cases} \tag{3.14}$$

where $a_{\alpha^+} = a_{(\alpha-1)^+} + \min(a_c - a_{(\alpha-1)^+}, \nu_\alpha C_\alpha N_d)$.

One may attempt to start the backward algorithm at time T_{α^-} with the payoff

$$u_{\alpha-1}(T_{\alpha^+}; a_{(\alpha-1)^+}) + \nu_\alpha L_d(T_\alpha) N_d - \nu_\alpha C_\alpha N_d. \tag{3.15}$$

However, there are several difficulties with this approach. First, (3.15) is a path-dependent payoff, similar to (3.7) arising in pricing knockout PRDC swaps. To overcome this difficulty, over each period of the tenor structure, we value the funding payment and the PRDC coupon parts separately, as we do when pricing knockout PRDC swaps, described in Subsection 3.5.

The second difficulty arises because the quantity

$$a_{\alpha^+} = a_{(\alpha-1)^+} + \min(a_c - a_{(\alpha-1)^+}, \nu_\alpha C_\alpha N_d)$$

needed to evaluate the right side of (3.13) may not be a gridpoint in the a-direction, i.e. not a gridpoint of the fixed set of points (3.11). As a result, the value

$$u_\alpha(T_{\alpha^+}; a_{\alpha^+}) \equiv u_\alpha(T_{\alpha^+}; a_{(\alpha-1)^+} + \min(a_c - a_{(\alpha-1)^+}, \nu_\alpha C_\alpha N_d))$$

of (3.14) may not be immediately available. Below, we illustrate how to enforce (3.14) using only the fixed set of gridpoints (3.11) for the a variable, and discuss the backward procedure for FX-TARN PRDC swaps from time T_{α^-} to $T_{(\alpha-1)^+}$ on a computational grid.

We denote by $u_\alpha(s^y_{\alpha,i}, r_{d,j}, r_{f,k}, t; a_y)$ an approximation to $u_\alpha(t; a_y)$ at the gridpoint $(s^y_{\alpha,i}, r_{d,j}, r_{f,k})$, where $\alpha = \beta, \ldots, 1$, $i = 1, \ldots, n$, $j = 1, \ldots, p$, $k = 1, \ldots, q$, and $y = 0, \ldots, w$. (Note that the quantity $u_0(T_0; 0) \equiv u_0(0; 0)$ corresponding to $(s(0), r_d(0), r_f(0))$ is an approximation to the value of the FX-TARN PRDC swap that we are interested in at time T_0, and can be obtained from $u_0(s^0_{1,i}, r_{d,j}, r_{f,k}, 0; 0)$. See Remark 3.7 for details.) For each T_α, we assume that the quantities $u_\alpha(s_{\alpha,i}, r_{d,j}, r_{f,k}, T_{\alpha^+}, a_y)$, $y = 0, \ldots, w$, are computed at the previous time period of the tenor structure, i.e. these are available at T_{α^+}.

On a computational grid, to enforce (3.14), we proceed as follows. For each a_y, $y = 0, \ldots, w$, and for each gridpoint $(s^y_{\alpha,i}, r_{d,j}, r_{f,k})$, we first find the corresponding quantity $\bar{a}_y$ specified by

$$\bar{a}_y = a_y + \min(a_c - a_y, \nu_\alpha C_\alpha N_d).$$

Note that the quantity $\bar{a}_y$ depends on T_α and on the partitions, but, to simplify the notation, we do not indicate these dependencies. We then find $u_{\alpha-1}(s^y_{\alpha,i}, r_{d,j}, r_{f,k}, T_{\alpha^+}; \bar{a}_y)$ using $u_\alpha(s^y_{\alpha,i}, r_{d,j}, r_{f,k}, T_{\alpha^+}; a_y)$, $y = 0, \ldots, w+1$. More specifically, if $\bar{a}_y \geq a_c$, the swap terminates pre-maturely at time T_α, whence $u_{\alpha-1}(s^y_{\alpha,i}, r_{d,j}, r_{f,k}, T_{\alpha^+}; \bar{a}_y)$ is zero. On the other hand, if $\bar{a}_y < a_c$, the swap does not terminate pre-maturely at time T_α. In this case, $\bar{a}_y$ may fall between two computational gridpoints in the a-direction, i.e. $a_{\bar{y}} \leq \bar{a}_y \leq a_{\bar{y}+1}$ for some $\bar{y}$ in $\{0, \ldots, w\}$. In addition, it is important to note that, since the barriers b^y_α, $y = 0, \ldots, w+1$, are not the same, the non-uniform partitions Δ^y_α, $y = 0, \ldots, w+1$, are different, primarily in the region around the barrier. Thus, $s^y_{\alpha,i}$ may fall between the computational gridpoints of $\Delta^{\bar{y}}_\alpha$ and $\Delta^{\bar{y}+1}_\alpha$, i.e.

$$s^{\bar{y}}_{\alpha,\bar{i}} \leq s^y_{\alpha,i} \leq s^{\bar{y}}_{\alpha,\bar{i}+1} \quad \text{and} \quad s^{\bar{y}+1}_{\alpha,\bar{\bar{i}}} \leq s^y_{\alpha,i} \leq s^{\bar{y}+1}_{\alpha,\bar{\bar{i}}+1}$$

for some $\bar{i}$ and $\bar{\bar{i}}$ in $\{0, \ldots, n\}$. To approximate $u_{\alpha-1}(s^y_{\alpha,i}, r_{d,j}, r_{f,k}, T_{\alpha^+}; \bar{a}_y)$, we apply two-dimensional linear interpolation along the s- and a-directions, which can be viewed as obtained by successively applying the standard one-dimensional linear interpolation along each respective direction, using the following four values:

$$u_\alpha(s^{\bar{y}}_{\alpha,\bar{i}}, r_{d,j}, r_{f,k}, T_{\alpha^+}; a_{\bar{y}}), \quad u_\alpha(s^{\bar{y}}_{\alpha,\bar{i}+1}, r_{d,j}, r_{f,k}, T_{\alpha^+}; a_{\bar{y}}),$$

and

$$u_\alpha(s^{\bar{y}+1}_{\alpha,\bar{\bar{i}}}, r_{d,j}, r_{f,k}, T_{\alpha^+}; a_{\bar{y}+1}), \quad u_\alpha(s^{\bar{y}+1}_{\alpha,\bar{\bar{i}}+1}, r_{d,j}, r_{f,k}, T_{\alpha^+}; a_{\bar{y}+1}).$$

More specifically, by first applying two one-dimensional linear interpolations along the s-direction, we obtain the quantities

$$\begin{aligned} u_\alpha(s^y_{\alpha,i}, r_{d,j}, r_{f,k}, T_{\alpha^+}; a_{\bar{y}}) \approx {} & \frac{s^y_{\alpha,i} - s^{\bar{y}}_{\alpha,\bar{i}}}{s^{\bar{y}}_{\alpha,\bar{i}+1} - s^{\bar{y}}_{\alpha,\bar{i}}} u_\alpha(s^{\bar{y}}_{\alpha,\bar{i}+1}, r_{d,j}, r_{f,k}, T_{\alpha^+}; a_{\bar{y}}) \\ & + \frac{s^{\bar{y}}_{\alpha,\bar{i}+1} - s^y_{\alpha,i}}{s^{\bar{y}}_{\alpha,\bar{i}+1} - s^{\bar{y}}_{\alpha,\bar{i}}} u_\alpha(s^{\bar{y}}_{\alpha,\bar{i}}, r_{d,j}, r_{f,k}, T_{\alpha^+}; a_{\bar{y}}), \end{aligned} \quad (3.16)$$

and

$$u_\alpha(s^y_{\alpha,i}, r_{d,j}, r_{f,k}, T_{\alpha^+}; a_{\bar{y}+1}) \approx \frac{s^y_{\alpha,i} - s^{\bar{y}+1}_{\alpha,\bar{\bar{i}}}}{s^{\bar{y}+1}_{\alpha,\bar{\bar{i}}+1} - s^{\bar{y}+1}_{\alpha,\bar{\bar{i}}}} u_\alpha(s^{\bar{y}+1}_{\alpha,\bar{\bar{i}}+1}, r_{d,j}, r_{f,k}, T_{\alpha^+}; a_{\bar{y}+1}) + \frac{s^{\bar{y}+1}_{\alpha,\bar{\bar{i}}+1} - s^y_{\alpha,i}}{s^{\bar{y}+1}_{\alpha,\bar{\bar{i}}+1} - s^{\bar{y}+1}_{\alpha,\bar{\bar{i}}}} u_\alpha(s^{\bar{y}+1}_{\alpha,\bar{\bar{i}}}, r_{d,j}, r_{f,k}, T_{\alpha^+}; a_{\bar{y}+1}). \quad (3.17)$$

Then, by performing a linear interpolation along the a-direction using the two intermediate quantities defined in (3.16) and (3.17), we arrive at the following approximation to $u_{\alpha-1}(s^y_{\alpha,i}, r_{d,j}, r_{f,k}, T_{\alpha^+}; \bar{a}_y)$:[6]

$$u_{\alpha-1}(s^y_{\alpha,i}, r_{d,j}, r_{f,k}, T_{\alpha^+}; \bar{a}_y) \approx \frac{\bar{a}_y - a_{\bar{y}}}{a_{\bar{y}+1} - a_{\bar{y}}} u_\alpha(s^y_{\alpha,i}, r_{d,j}, r_{f,k}, T_{\alpha^+}; a_{\bar{y}+1}) + \frac{a_{\bar{y}+1} - \bar{a}_y}{a_{\bar{y}+1} - a_{\bar{y}}} u_\alpha(s^y_{\alpha,i}, r_{d,j}, r_{f,k}, T_{\alpha^+}; a_{\bar{y}}). \quad (3.18)$$

Note that, in the special case that $\bar{y} = w$, we set $u_\alpha(\cdot,\cdot,\cdot,T_{\alpha^+}; a_{\bar{y}+1}) \equiv u_\alpha(\cdot,\cdot,\cdot,T_{\alpha^+}; a_c) = 0$. The above procedure essentially enforces (3.14), within the accuracy of linear interpolation. A pictorial illustration of this two-dimensional linear interpolation procedure is given in Figure 3.3. Figure 3.4 presents an illustration of the procedure to enforce (i) the updating rules in (2.16) and (2.17) using only the fixed set of gridpoints (3.11) for the a variable, and (ii) a possibility of early termination at each date of the swap's tenor structure.

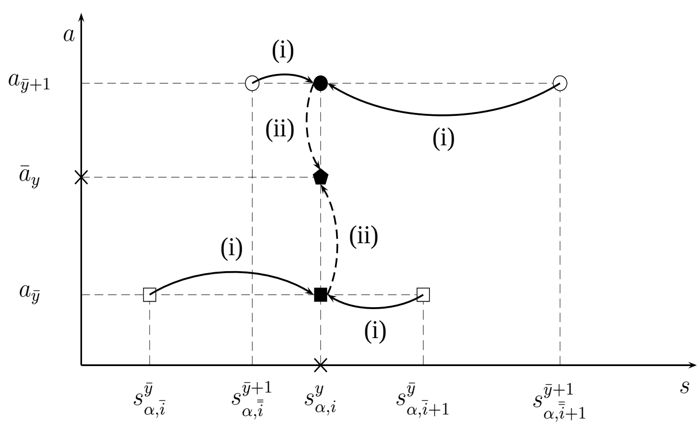

Figure 3.3: A two-dimensional linear interpolation procedure to enforce (3.14) which can be viewed as obtained by combining linear interpolations along (i) the s-direction (see (3.16) and (3.17)), and (ii) the a-direction (see (3.18)).

In implementing the backward procedure, we first take into account the PRDC coupon payment by computing

$$u^{(1)}_{\alpha-1}(s^y_{\alpha,i}, r_{d,j}, r_{f,k}, T_{\alpha^-}; a_y) = u_{\alpha-1}(s^y_{\alpha,i}, r_{d,j}, r_{f,k}, T_{\alpha^+}; \bar{a}_y) - \min(a_c - a_y, \nu_\alpha C_\alpha N_d), \quad y = 0, \ldots, w,$$

which becomes the terminal condition for the PDE (2.10). We next solve this PDE backward in time from T_{α^-} to $T_{(\alpha-1)^+}$ using the ADI scheme (3.5) for each time τ_m, $m = 1, \ldots, l$, to obtain

$$u^{(2)}_{\alpha-1}(s^y_{\alpha,i}, r_{d,j}, r_{f,k}, T_{(\alpha-1)^+}; a_y).$$

[6] When the spatial partitions are the same for all a_y's, the procedure described above simplifies to one-dimensional linear interpolation along the s-direction [43].

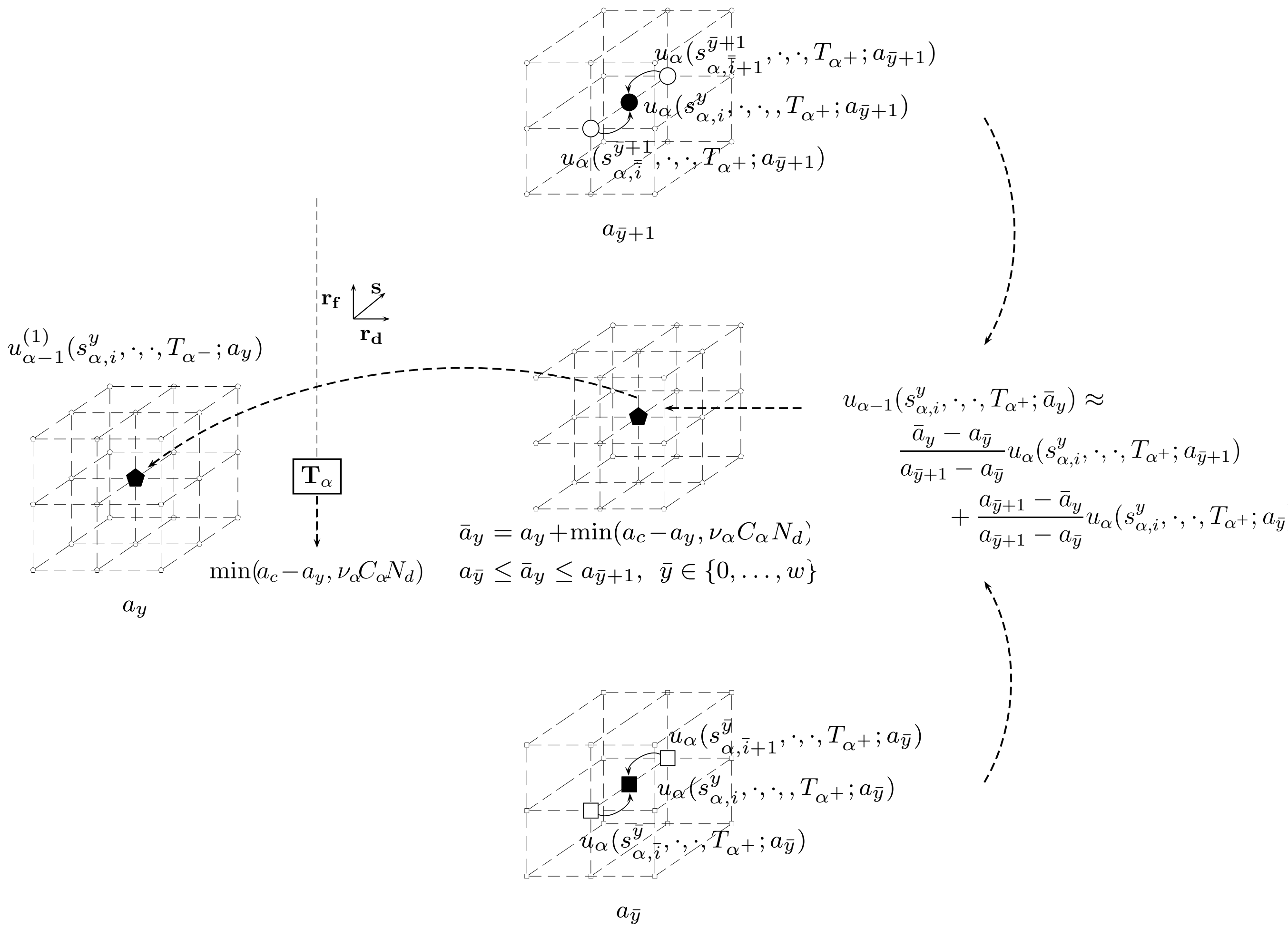

Figure 3.4: A procedure to enforce (i) the updating rules in (2.16) and (2.17) using only the fixed set of gridpoints (3.11) for the a variable and (ii) a possibility of early termination at each date of the swap's tenor structure.

Then, we interpolate $u^{(2)}_{\alpha-1}(s^{y}_{\alpha,i}, r_{d,j}, r_{f,k}, T_{(\alpha-1)^+}; a_y)$ to obtain $u^{(3)}_{\alpha-1}(s^{y}_{\alpha-1,i}, r_{d,j}, r_{f,k}, T_{(\alpha-1)^+}; a_y)$. Finally, we incorporate the funding leg payment by computing

$$u_{\alpha-1}(s^{y}_{\alpha-1,i}, r_{d,j}, r_{f,k}, T_{(\alpha-1)^+}; a_y) = u^{(3)}_{\alpha-1}(s^{y}_{\alpha-1,i}, r_{d,j}, r_{f,k}, T_{(\alpha-1)^+}; a_y) + (1 - P_d(T_\alpha))N_d.$$

A backward pricing algorithm for FX-TARN PRDC swaps is presented in Algorithm 3.4.

REMARK 3.6. To improve the accuracy of the interpolation scheme (3.18) enforcing (3.14), for the a variable, we use non-uniform partitions that are more concentrated towards the cap a_c, due to possible discontinuities in the swap values at a_c. Such non-uniform partitions can be constructed using Algorithm 3.1 with settings as discussed in Remark 3.1.

REMARK 3.7. Note that, since $s(0)$ is not guaranteed to be a gridpoint of Δ^0_1, interpolation along the s-direction may be needed to compute an approximation to $u_0(0; 0)$ corresponding to $(s(0), r_d(0), r_f(0))$ using the values $u_0(s^0_{1,i}, r_{d,j}, r_{f,k}, 0; 0)$, $i = 0, \ldots, n+1$. To avoid this possible interpolation, we adjust the partition Δ^0_1 as noted in Remark 3.4 for knockout PRDC swaps.

Algorithm 3.4 Backward algorithm for computing FX-TARN PRDC swaps.

construct Δ_β^y by Algorithm (3.2), and set $u_\beta(\cdot,\cdot,\cdot,T_{\beta^+};a_y)=0$, $y=0,\ldots,w$;
for $\alpha=\beta,\ldots,1$ **do**
  for each a_y, $y=0,\ldots,w$, **do**
    set
$$\bar{a}_y = a_y + \min(a_c - a_y, \nu_\alpha C_\alpha N_d); \tag{3.19}$$
    set
$$u_{\alpha-1}(s^y_{\alpha,i}, r_{d,j}, r_{f,k}, T_{\alpha^+}; \bar{a}_y) = \begin{cases} 0 & \text{if } \bar{a}_y \geq a_c, \\ \dfrac{\bar{a}_y - a_{\bar{y}}}{a_{\bar{y}+1} - a_{\bar{y}}} u_\alpha(s^y_{\alpha,i}, r_{d,j}, r_{f,k}, T_{\alpha^+}; a_{\bar{y}+1}) & \\ \quad + \dfrac{a_{\bar{y}+1} - \bar{a}_y}{a_{\bar{y}+1} - a_{\bar{y}}} u_\alpha(s^y_{\alpha,i}, r_{d,j}, r_{f,k}, T_{\alpha^+}; a_{\bar{y}}) & \text{if } a_{\bar{y}} \leq \bar{a}_y \leq a_{\bar{y}+1}, \\ & \quad \bar{y} \in \{0,\ldots,w\}, \end{cases} \tag{3.20}$$
    where $u_\alpha(s^y_{\alpha,i}, r_{d,j}, r_{f,k}, T_{\alpha^+}; a_{\bar{y}})$ and $u_\alpha(s^y_{\alpha,i}, r_{d,j}, r_{f,k}, T_{\alpha^+}; a_{\bar{y}+1})$ are defined by (3.16) and (3.17), respectively;
    set
$$u^{(1)}_{\alpha-1}(s^y_{\alpha,i}, r_{d,j}, r_{f,k}, T_{\alpha^-}; a_y) = u_{\alpha-1}(s^y_{\alpha,i}, r_{d,j}, r_{f,k}, T_{\alpha^+}; \bar{a}_y) - \min(a_c - a_y, \nu_\alpha C_\alpha N_d); \tag{3.21}$$
    solve the PDE (2.10) with the terminal condition (3.21) from T_{α^-} to $T_{(\alpha-1)^+}$ using the ADI scheme (3.5) for each time τ_m, $m=1,\ldots,l$, with the timestep size $\Delta\tau_m$ selected by (3.6), to obtain $u^{(2)}_{\alpha-1}(s^y_{\alpha,i}, r_{d,j}, r_{f,k}, T_{(\alpha-1)^+}; a_y)$;
    if $\alpha \geq 2$ **then**
      construct $\Delta^y_{\alpha-1}$ by Algorithm (3.2);
      interpolate $u^{(2)}_{\alpha-1}(s^y_{\alpha,i}, r_{d,j}, r_{f,k}, T_{(\alpha-1)^+}; a_y)$ to obtain $u^{(3)}_{\alpha-1}(s^y_{\alpha-1,i}, r_{d,j}, r_{f,k}, T_{(\alpha-1)^+}; a_y)$;
      set $u_{\alpha-1}(s^y_{\alpha-1,i}, r_{d,j}, r_{f,k}, T_{(\alpha-1)^+}; a_y) = u^{(3)}_{\alpha-1}(s^y_{\alpha-1,i}, r_{d,j}, r_{f,k}, T_{(\alpha-1)^+}; a_y) + (1-P_d(T_\alpha))N_d$;
    else
      set $u_{\alpha-1}(s^y_{\alpha,i}, r_{d,j}, r_{f,k}, T_{(\alpha-1)^+}; a_y) = u^{(2)}_{\alpha-1}(s^y_{\alpha,i}, r_{d,j}, r_{f,k}, T_{(\alpha-1)^+}; a_y) + (1-P_d(T_\alpha))N_d$;
    end if
  end for
end for
set $u_0(\cdot,\cdot,\cdot,T_0;0) = u_0(\cdot,\cdot,\cdot,T_{0^+};0)$;

3.6.4. Other versions of FX-TARN PRDC swaps

The above algorithm for pricing the first version of FX-TARN PRDC swaps could, after straight-forward modifications, be used for pricing the second and third versions of the FX-TARN. Recall that, for all three versions of the FX-TARN PRDC swaps, the target cap a_c is fixed and known in advance, and the only difference between the first version and the second and third versions of the FX-TARN PRDC swaps is how the PRDC coupon amount scheduled on the early termination date is handled. As a result, we can use the same discretization for the a variable via the set of fixed gridpoints (3.11), and, in the pricing algorithm, we only need to adjust the actual PRDC coupon amount paid at each date T_α, $\alpha = \beta, \ldots, 1$, to be

$$\min(a_y, \nu_\alpha C_\alpha N_d) \quad \text{and} \quad \nu_\alpha C_\alpha N_d$$

for the second and third versions of the FX-TARN PRDC swaps, respectively.

3.7. Overview of a parallelization of the pricing algorithms

To design a parallel algorithm, we divide the pricing of FX-TARN PRDC swaps into $w + 1$ independent pricing sub-problems, one for each gridpoint, a_y, $y = 0, 1, \ldots, w$, of the a-grid, during each period, $[T_{(\alpha-1)^+}, T_{\alpha^-}]$, of the tenor structure. We can run these $w + 1$ pricing processes in parallel on each period of the tenor structure, with communication only at $\{T_\alpha\}_{\alpha=1}^{\beta-1}$, where exchange of data is required between the processes to implement the interpolation scheme (3.18). Our implementation of Algorithm 3.4 uses a cluster of Graphics Processing Units (GPUs) together with the Compute Unified Device Architecture (CUDA) Application Programming Interface to solve these $w + 1$ independent sub-problems simultaneously, each on a separate GPU. A second level of parallelism can be exploited, since the main computational task associated with each sub-problem is the solution of the model PDE (2.10), which can be accomplished via a highly efficient GPU-based parallelization of the ADI timestepping technique (3.5a)–(3.5d), details of which can be found in [13]. In addition, we utilize the Message Passing Interface (MPI) [20, 21], a widely used message passing library standard, for efficient communication between the pricing processes at the end of each time period, i.e. at $\{T_\alpha\}_{\alpha=1}^{\beta-1}$. Details of an implementation of Algorithm 3.4 on a GPU cluster and selected timing results for knockout and FX-TARN PRDC swaps can be found in [12].

4. Numerical results

4.1. Model parameters

As parameters to the model, we consider the same interest rates, correlation parameters, and the local volatility function as given in [34]. The domestic (JPY) and foreign (USD) interest rate curves are given by $P_d(0, T) = \exp(-0.02 \times T)$ and $P_f(0, T) = \exp(-0.05 \times T)$. The volatility parameters for the short rates and correlations are given by $\sigma_d(t) = 0.7\%$, $\kappa_d(t) = 0.0\%$, $\sigma_f(t) = 1.2\%$, $\kappa_f(t) = 5.0\%$, $\rho_{df} = 25\%$, $\rho_{ds} = -15\%$, $\rho_{fs} = -15\%$. The initial spot FX rate is set to $s(0) = 105.00$, and the initial domestic and foreign short rate are 0.02 (2%) and 0.05 (5%), respectively, which follows from the respective interest rate curve. The parameters $\xi(t)$ and $\varsigma(t)$ for the local volatility function are assumed to be piecewise constant and given in Table 4.1. Note that the forward FX rate $F(0, t)$ defined by (2.5) and $\theta_i(t)$, $i = d, f$, in (2.8), and the

	period (years)									
	(0, 0.5]	(0.5, 1]	(1, 3]	(3, 5]	(5, 7]	(7, 10]	(10, 15]	(15, 20]	(20, 25]	(25, 30]
$\xi(t)$	9.03%	8.87%	8.42%	8.99%	10.18%	13.30%	18.18%	16.73%	13.51%	13.51%
$\varsigma(t)$	-200%	-172%	-115%	-65%	-50%	-24%	10%	38%	38%	38%

Table 4.1: The parameters $\xi(t)$ and $\varsigma(t)$ for the local volatility function (2.9). (Table C in [34].)

domestic LIBOR rate (2.3) are fully determined by the above information [1, 4].

We consider the tenor structure (2.1) that has the following properties: (i) $\nu_\alpha = 1$ (year), $\alpha = 1, \ldots, \beta+1$ and (ii) $\beta = 29$ (years). Features of the PRDC swap are:

- Pay annual PRDC coupons and receive annual domestic LIBOR payments.

- Standard structure, i.e. $b_f = 0$, $b_c = +\infty$. The scaling factor $\{f_\alpha\}_{\alpha=1}^{\beta}$ is set to the forward FX rate $F(0, T_\alpha)$.
- The domestic and foreign coupons are chosen to provide three different levels of leverage: low ($c_d = 2.25\%, c_f = 4.50\%$), medium ($c_d = 4.36\%, c_f = 6.25\%$), high ($c_d = 8.1\%, c_f = 9.00\%$).
- Exotic features:

  - Knockout: the fixed upper barrier is set to $b = 110.25$, 120.75 and 131.25 for the low-, medium- and high-leverage levels, respectively.

  - FX-TARN: the cap a_c is set to $a_c = 50\%$, 20%, and 10% of the notional for the low-, medium-, and high-leverage levels, respectively.

The truncated computational domain Ω is defined by setting $s_\infty = 5s(0) = 525.0$, $r_{d,\infty} = 10r_d(0) = 0.2$, and $r_{f,\infty} = 10r_f(0) = 0.5$. The grid sizes and the number of timesteps reported in the tables in this section are for each time period of the Table 4.1. Note that, when the timestep size selector (3.6) is used, the number of timesteps reported is the average number of timesteps over all time periods of the swap's tenor structure.

We report the quantity "value", which is the value of the financial instrument. In pricing PRDC swaps, this quantity is expressed as a percentage of the notional N_d. Since in our case, an accurate reference solution is not available, to provide an estimate of the convergence rate of the algorithm, we also compute the quantity "$\log_\eta$ ratio" which provides an estimate of the convergence rate of the algorithm by measuring the differences in prices on successively finer grids, referred to as "change". More specifically, this quantity is defined by

$$\log_\eta \text{ratio} = \log_\eta \left(\frac{u_{approx}(\Delta x) - u_{approx}(\frac{\Delta x}{\eta})}{u_{approx}(\frac{\Delta x}{\eta}) - u_{approx}(\frac{\Delta x}{\eta^2})} \right),$$

where $u_{approx}(\Delta x)$ is the approximate solution computed with discretization stepsize Δx. For second-order methods, the quantity $\log_\eta$-ratio is expected to be about 2. As demonstrated further in this section, the methods in this paper exhibit second-order convergence, even if the non-uniform grids constructed may not be smooth at a few points.

REMARK 4.1. It is important to note that, in the first time period, $[0, 1]$, of the swap's tenor structure, the piecewise constant parameters $\xi(t)$ and $\varsigma(t)$ of the local volatility function change their values at the time $t = 0.5$ (see Table 4.1). As a result, when solving the model PDE in the first time period $[0, 1]$, it is desirable to make the time $t = 0.5$ a gridpoint in the time direction to avoid a non-smooth change in the coefficients of the model PDE within one timestep.

4.2. Non-uniform spatial partitions

The non-uniform partitions for the domestic and foreign short rates, r_d and r_f, respectively, are constructed using the procedure *PartitionOne*(l, u, c, e, i, d_l, d_u) described in Algorithm 3.1. More specifically, as input to this procedure, for the r_d variable, we use $l = -r_{d,\infty}$, $u = r_{d,\infty}$, $d_l = d_u = 0.0005$. The index i of the point of interest, $r_d(0)$, is set to $i = \texttt{ceil}(0.4(p+1))$. For the r_f variable, we use the same set of parameters, except for $l = -r_{f,\infty}$, $u = r_{f,\infty}$ and $i = \texttt{ceil}(0.4(q+1))$. (Note that the total numbers of sub-intervals are $p+1$ and $q+1$ for r_d and r_f, respectively.) An example of such non-uniform partitions with $p = q = 40$ is given in Figure 4.1. Note that the partitions for both interest short rates are the same for all time periods of the swap's tenor structure.

The strike k_α, $\alpha = 29, \ldots, 1$, can be computed via (2.6), with the forward FX rate $F(0, t)$ (2.5) being fully determined by the model parameters. For a knockout PRDC swap, the non-uniform partition Δ_α is

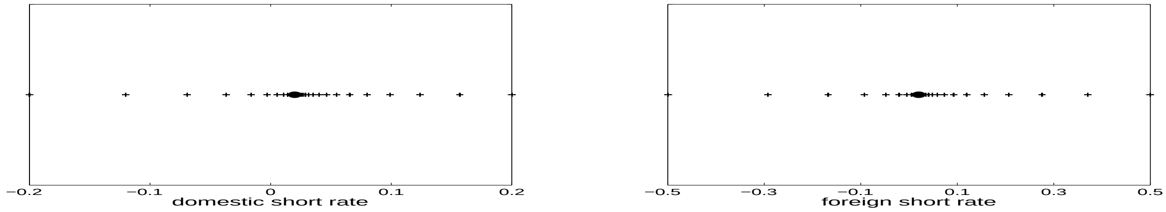

(a) (b)

Figure 4.1: The location of the gridpoints for the non-uniform partitions for the domestic (a) and foreign (b) interest short rate variables. The points of interest, $r_d(0)$ and $r_f(0)$, which are the instantaneous forward rates, are each marked by a black dot.

first constructed using the procedure *PartitionMulti*($L, U, \{c_j\}_{j=1}^{2}, \{e_j\}_{j=1}^{2}, \{i_j\}_{j=1}^{2}, \{d_l^j\}_{j=1}^{2}, \{d_u^j\}_{j=1}^{2}$) as described in Algorithm 3.2. We then apply the adjustment described in Remark 3.3 to ensure that b falls at a midpoint. As input to the partition generating procedure, for all time periods of the swap's tenor structure, we use the set of parameters listed in Table 4.2. Examples of such non-uniform partitions with $n = 35$ are given in Figures 4.2 (a) and (b) .

	L	U	c_1	c_2	e_1	e_2	i_1	i_2	d_l^1	d_l^2	u_l^1	u_l^2
	knockout											
Algorithm 3.2	0	s_∞	k_α	b	$\texttt{ceil}(\frac{n+1}{2})$	$(n+1) - e_1$	$\texttt{ceil}(0.5e_1)$	$\texttt{ceil}(0.4e_2)$	10	10	10	3.5
	FX-TARN											
Algorithm 3.1 (the a variable)	0	a_c	a_c	n/a	$w+1$	n/a	e_1	n/a	0.01	n/a	n/a	n/a
Algorithm 3.2	0	s_∞	k_α	b_α^y	$\texttt{ceil}(\frac{n+1}{2})$	$(n+1) - e_1$	$\texttt{ceil}(0.5e_1)$	$\texttt{ceil}(0.4e_2)$	10	10	10	3.5
Algorithm 3.1 ($b_\alpha^y - k_\alpha < 15$)	0	s_∞	k_α	n/a	$n+1$	n/a	$\texttt{ceil}(0.5e_1)$	n/a	10	n/a	10	n/a

Table 4.2: Parameters to the partition generating procedures *PartitionOne* (Algorithm 3.1) and *PartitionMulti* (Algorithm 3.2) employed to generate non-uniform partitions for the s and a variables. Here, the total numbers of sub-intervals are $n+1$ and $w+1$ for the s and a variables, respectively.

For a FX-TARN PRDC swap, the non-uniform partition for the a variable is constructed using the procedure *PartitionOne* with modifications as described in Remark 3.1. The parameters for this procedure are given in Table 4.2. For each a_y, $y = 0, \ldots, w$, of the partition for the a variable constructed in this fashion and for each T_α, $\alpha = 29, \ldots, 1$, the non-uniform partition Δ_α^y for the s variable can be generated using *PartitionMulti* in a similar fashion to those constructed for a knockout PRDC swap. However, we switch to procedure *PartitionOne* when $b_\alpha^y - k_\alpha <$ `small-range` (see Remark 3.5). As input to the partition generating procedure, for all time periods of the swap's tenor structure and for all a_y, we use the set of parameters listed in Table 4.2. Examples of such non-uniform partitions with $n = 35$ and several different values of a_y are given in Figures 4.2 (c) and (d). It may be interesting to investigate further possibly better parameter settings for the partition generating procedures. However, this is beyond the scope of this paper.

4.3. Numerical results

4.3.1. Convergence and efficiency

In this subsection, we discuss the convergence of the computed prices and the efficiency of the numerical methods developed in this paper for knockout and FX-TARN PRDC swaps. An analysis of the pricing results

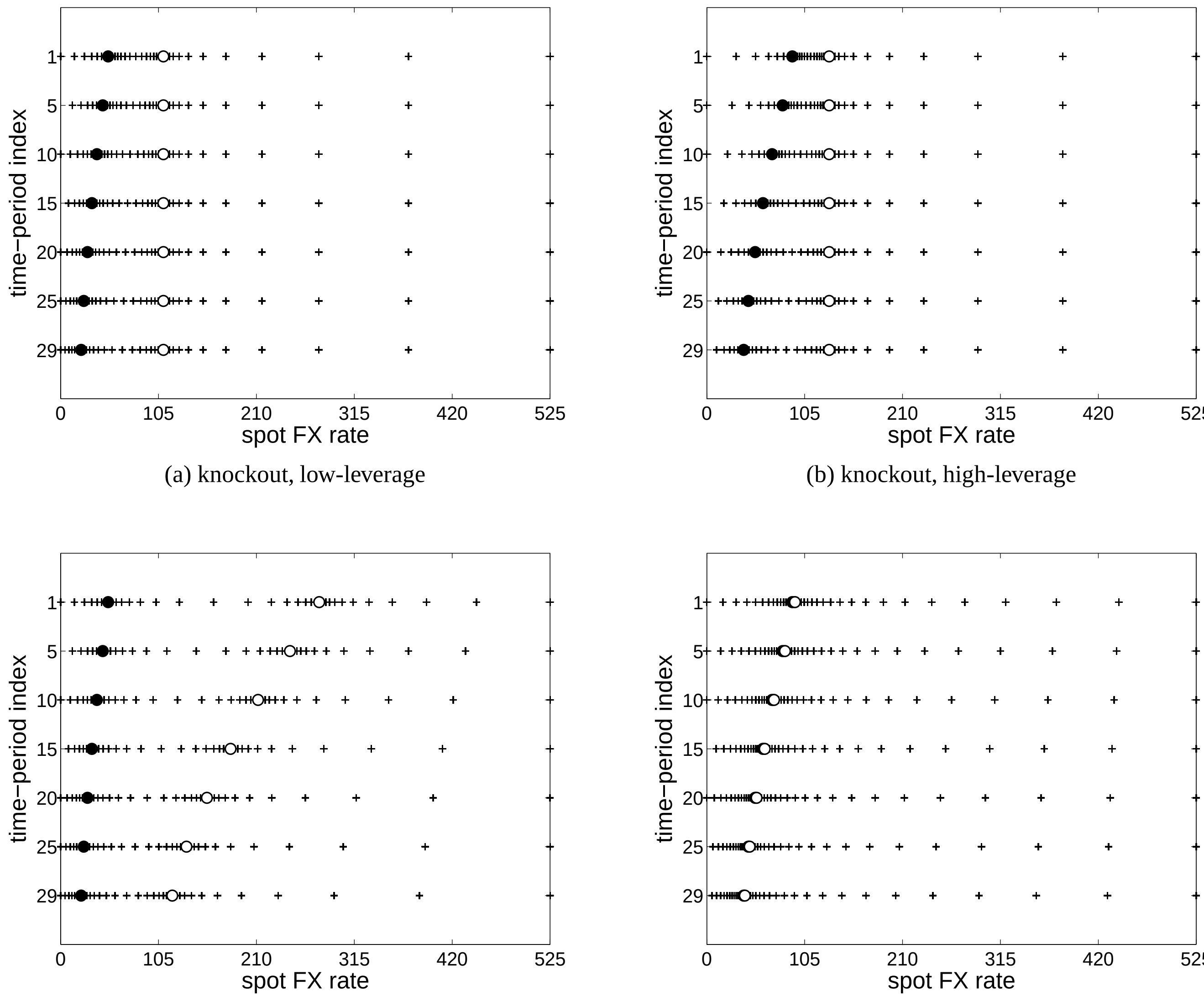

(a) knockout, low-leverage

(b) knockout, high-leverage

(c) FX-TARN, high-leverage ($a_c = 10\%$), $a_y = 0\%$

(d) FX-TARN, high-leverage ($a_c = 10\%$), $a_y \approx 9.70\%$

Figure 4.2: The location of the gridpoints of the non-uniform partitions for the s variable at selected dates of the swap's tenor structure used for pricing a knockout PRDC swap with low-leverage coupon (a) and high-leverage coupon (b), and for a high-leverage FX-TARN PRDC swap with $a_y = 0\%$ (c) and $a_y \approx 9.70\%$ (d). The strike k_α is marked by a black dot, while the barrier is marked by a white dot.

is given in the next subsection. In addition to the ADI-FD method with non-uniform grids and timestep sizes chosen by (3.6) (non-uniform ADI-FD) described in this paper, we also carried out experiments with the ADI-FD method with uniform grids and uniform timestep sizes (uniform ADI-FD).

Note that, with the above choice of the truncated computational domain and for all spatial grid sizes considered for the ADI-FD uniform method, there is a gridpoint at the spot value in each spatial dimension, i.e. at $s(0)$, $r_d(0)$ and $r_f(0)$. Also, for all grid sizes considered for the knockout PRDC swaps with uniform grids, the fixed FX-linked barrier b is one of the midpoints of the grid in the spot FX rate direction, i.e. we use the grid shifting strategy.

a) Knockout PRDC swaps

In the left half of Table 4.3, under the header “with grid shifting”, we present pricing results for the knockout PRDC swap for various leverage levels obtained using the uniform ADI-FD method and the grid shifting technique. Note that, when uniform grids are used, tripling the number of gridpoints ($\eta = 3$) of a coarser grid having the fixed FX-linked barrier b as a midpoint ensures that the resulting finer grid has the same property. We expect the quantity $\log_3$ ratio to be about 2 for a second-order discretization method as the grids are refined in this fashion. When the grid shifting technique is employed, the computed prices indicate second-order convergence is achieved for the uniform ADI-FD method, as expected.

leverage level	l (τ)	$n{+}1$ (s)	$p{+}1$ (r_d)	$q{+}1$ (r_f)	value (%)	change	$\log_3$ ratio	l (τ)	$n{+}1$ (s)	$p{+}1$ (r_d)	$q{+}1$ (r_f)	value (%)	change	$\log_2$ ratio
	with grid shifting							without grid shifting						
low	6	50	40	40	0.856			12	100	80	80	0.841		
	18	150	120	120	1.321	4.6e-03		24	200	160	160	1.107	2.7e-03	
	54	450	360	360	1.358	4.7e-04	2.2	48	400	320	320	1.241	1.3e-03	1.1
medium	6	50	40	40	1.441			12	100	80	80	1.416		
	18	150	120	120	2.049	6.1e-03		24	200	160	160	1.768	3.5e-03	
	54	450	360	360	2.109	5.9e-04	2.1	48	400	320	320	1.943	1.7e-03	1.0
high	6	50	40	40	5.104			12	100	80	80	4.837		
	18	150	120	120	5.468	3.6e-03		24	200	160	160	5.183	3.4e-03	
	54	450	360	360	5.519	4.8e-04	1.9	48	400	320	320	5.354	1.7e-03	1.1

Table 4.3: Computed prices and convergence results for the knockout PRDC swap for various leverage levels under the FX skew model obtained using the uniform ADI-FD method. HV smoothing is applied.

To show the effect of the grid shifting technique on the convergence and accuracy of the numerical methods, we carried out experiments with different uniform grids which do not have b as a midpoint, but rather as a gridpoint, in the spot FX rate direction. The results of these experiments are presented in the right half of Table 4.3 under the header “without grid shifting”. In these experiments, the coarser grids having the fixed FX-linked barrier b as a gridpoint are refined by doubling the number of gridpoints ($\eta = 2$). It is evident from Table 4.3 that, although the prices obtained by the uniform ADI-FD method without grid shifting appear to converge to the approximately same values as those obtained by the uniform ADI-FD method with grid shifting, only linear convergence is observed in this case, i.e. the observed $\log_2$ ratio is about 1 instead of 2. This emphasizes the importance of handling appropriately the discontinuities in the terminal conditions on each date of the tenor structure of the knockout PRDC swaps, as discussed in Remark 3.2.

In Table 4.4, we report the pricing results for knockout PRDC swaps for various leverage levels obtained using the non-uniform ADI-FD method. Note that, our approach to constructing non-uniform grids ensures that the grid shifting technique is always employed. The computed prices indicate that second-order convergence is achieved for the non-uniform ADI-FD method when applied to knockout PRDC swaps.

b) FX-TARN PRDC swaps

In Table 4.5, we present pricing results for FX-TARN PRDC swaps for various levels of leverage and values of the target cap a_c obtained with uniform and non-uniform ADI-FD methods. In all cases, the number of sub-intervals in the a-direction is 40, i.e. $w = 39$ in (3.11). Hence, 40 pricing sub-problems must be solved over each time period of the swap's tenor structure. Observe that, similar to knockout PRDC swaps, for all leverage levels, the computed prices also exhibit second-order convergence, as expected from the ADI timestepping methods and the interpolation scheme.

leverage level	l (τ)	$n+1$ (s)	$p+1$ (r_d)	$q+1$ (r_f)	value (%)	change	$\log_2$ ratio
low	5	40	20	20	1.195		
	11	80	40	40	1.328	1.3e-3	
	22	160	80	80	1.358	3.0e-4	2.1
	43	320	160	160	1.365	6.8e-5	2.0
medium	5	40	20	20	1.996		
	11	80	40	40	2.091	9.5e-4	
	22	160	80	80	2.110	1.9e-4	2.3
	43	320	160	160	2.115	5.4e-5	1.9
high	5	40	20	20	5.364		
	11	80	40	40	5.490	1.2e-3	
	22	160	80	80	5.516	2.6e-4	2.2
	43	320	160	160	5.523	6.9e-5	1.9

Table 4.4: Computed prices and convergence results for knockout PRDC swaps for various leverage levels under the FX skew model using the non-uniform ADI-FD method. Grid shifting technique is embedded. HV smoothing is applied.

As mentioned in Subsection 2.2, using artificial boundary conditions may induce additional approximation errors into the numerical solutions. However, we can make these errors sufficiently small by choosing sufficiently large values for $s = s_\infty$, $r_{d,\infty}$, and $r_{f,\infty}$. Table 4.6 shows select prices of high-leverage PRDC swaps obtained with different large boundaries. The spatial and timestep sizes in these examples are chosen to be the same with those of the coarsest grids in Tables 4.3 (with grid shifting) and 4.5a. It is observed that, smaller range for the truncated boundary values $s = s_\infty$, $r_{d,\infty}$, and $r_{f,\infty}$ than what we use in this paper may be inappropriate, since the computed prices of the swaps appear to be sensitive to these values of the boundaries. However, once these values are sufficiently large, we do not observed sensitivities in the computed prices of the swaps to boundaries of the computational domain.

We conclude this subsection by noting that second-order convergence on non-uniform grids of various ADI FD schemes, including the HV scheme considered in this paper, applied to the three-dimensional PDE arising from the hybrid Heston-Hull-White model [23, 24] has been recently reported in [22]. However, the non-uniform spatial partitions considered in our paper have two concentration points, as opposed to those with only one concentration point used in [22].

c) Discussion of efficiency

To check the accuracy and to compare the efficiency between the uniform and non-uniform ADI-FD methods, we establish benchmark prices for knockout/FX-TARN swaps for different leverage levels using MC simulations. With 10^6 simulation paths for the spot FX rate, the timestep size being $1/512$ of a year, and using antithetic variates as the variance reduction technique, for the low-, medium-, and high-leverage levels, the benchmark prices for the knockout PRDC swap are 1.368% (with standard deviation (std. dev.) = 0.016), 2.116% (std. dev. = 0.015), and 5.526% (std. dev. = 0.019), respectively. The 95% confidence intervals (CIs) are $[1.364\%, 1.371\%]$, $[2.113\%, 2.119\%]$ and $[5.522\%, 5.530\%]$, respectively, For the FX-TARN PRDC swap, the MC benchmark prices and the 95% CIs are -4.383% (std. dev. = 0.020, 95% CI = [-4.386%, -4.379%]), 3.796% (std. dev. = 0.018, 95% CI = [3.792%, 3.799%]), and 18.638% (std. dev. = 0.021, 95% CI = [18.635%, 18.641%]), respectively. Each of the 95% CIs contains the respective PDE-computed swap

leverage level	a_c	$w+1$ (a)	l (τ)	$n{+}1$ (s)	$p{+}1$ (r_d)	$q{+}1$ (r_f)	value $(\%)$	change	$\log_2$ ratio
			6	60	40	40	-4.691		
low	50%	40	12	120	80	80	-4.467	2.2e-03	
			24	240	160	160	-4.405	6.2e-04	1.9
			48	480	160	160	-4.388	1.7e-04	1.9
			6	60	40	40	3.402		
medium	20%	40	12	120	80	80	3.692	2.9e-03	
			24	240	160	160	3.768	7.5e-04	1.9
			48	480	160	160	3.787	2.0e-04	1.9
			6	60	40	40	18.212		
high	10%	40	12	120	80	80	18.528	3.1e-03	
			24	240	160	160	18.610	8.1e-04	1.9
			48	480	160	160	18.631	2.1e-04	1.9

(a) uniform ADI-FD

leverage level	a_c	$w+1$ (a)	l (τ)	$n{+}1$ (s)	$p{+}1$ (r_d)	$q{+}1$ (r_f)	value $(\%)$	change	$\log_2$ ratio
			6	30	15	15	-4.487		
low	50%	30	12	60	30	30	-4.409	7.8e-04	
			23	120	60	60	-4.389	2.0e-04	1.9
			47	240	120	120	-4.384	5.4e-05	1.9
			6	30	15	15	3.709		
medium	20%	30	12	60	30	30	3.775	6.5e-04	
			23	120	60	60	3.789	1.4e-04	2.0
			47	240	120	120	3.793	3.8e-05	1.9
			6	30	15	15	18.521		
high	10%	30	12	60	30	30	18.609	8.8e-04	
			23	120	60	60	18.631	2.2e-04	1.9
			47	240	120	120	18.637	5.9e-05	1.9

(b) non-uniform ADI-FD

Table 4.5: Values of the FX-TARN PRDC swap for various leverage levels under the FX skew model. HV smoothing is applied.

price.

Due to memory limitations, we were not able to compute prices on an uniform mesh finer than the finest one in Tables 4.3 (with grid shifting) and 4.5(a). As a consistency check, we compared the MC benchmark prices with the prices obtained using the computed prices in these two tables and extrapolation, assuming quadratic convergence, since the uniform ADI-FD method is supposed to achieve this. With an accuracy requirement 10^{-5}, for the low-, medium-, and high-leverage levels, the extrapolated prices for the knockout PRDC swap obtained by the uniform ADI-FD method are 1.367%, 2.118%, and 5.525%, respectively. For the FX-TARN PRDC swap, the extrapolated prices are -4.381%, 3.795%, and 18.638%, respectively. All these extrapolated prices all agree very well with the MC prices and the 95% CIs.

As observed in Tables 4.3, 4.4 and 4.5, for both the knockout and FX-TARN PRDC swaps, the computed prices obtained by the non-uniform ADI-FD method converge to the benchmark prices more quickly than

$[0, s_\infty] \times [-r_{d,\infty}, r_{d,\infty}] \times [-r_{f,\infty}, r_{f,\infty}]$	l (τ)	$n{+}1$ (s)	$p{+}1$ (r_d)	$q{+}1$ (r_f)	value (%)
	uniform ADI-FD (knockout)				
$[0, 315] \times [-0.1, 0.1] \times [-0.25, 0.25]$	6	30	40	40	0.853
$[0, 1050] \times [-0.5, 0.5] \times [-0.75, 0.75]$	6	100	200	120	0.856
$[0, 2100] \times [-1.0, 1.0] \times [-1.0, 1.0]$	6	200	400	160	0.856
	uniform ADI-FD (FX-TARN)				
$[0, 315] \times [-0.1, 0.1] \times [-0.25, 0.25]$	6	36	40	40	-4.708
$[0, 1050] \times [-0.5, 0.5] \times [-0.75, 0.75]$	6	120	200	120	-4.691
$[0, 2100] \times [-1.0, 1.0] \times [-1.0, 1.0]$	6	240	400	160	-4.691

Table 4.6: Effect of finite boundary. Low-leverage level.

do the prices obtained by the uniform ADI-FD method. In addition, it is also evident from these tables that the non-uniform ADI-FD method is substantially more efficient than its uniform counterpart when applied to price knockout and FX-TARN PRDC swaps. As an illustrative example, for the knockout swap, compare the uniform ADI-FD method with $(n+1) \times (p+1) \times (q+1) \times l \equiv 150 \times 120 \times 120 \times 18$ in Table 4.3 (with grid shifting), to the non-uniform ADI-FD method with $(n+1) \times (p+1) \times (q+1) \times l \equiv 80 \times 40 \times 40 \times 11$ in Table 4.4. It is evident that, for all leverage levels, the non-uniform ADI-FD method is more accurate than its uniform counterpart (compare 1.328%, 2.091%, and 5.490% in Table 4.4 to 1.321% 2.049% and 5.468% in Table 4.3 (with grid shifting), respectively), while using only about 6% ($\approx \frac{80\times40\times40}{150\times120\times120}$) of the total number of gridpoints and about 61% ($\approx \frac{12}{18}$) of the total number of timesteps. Similar efficiency results hold for the FX-TARN PRDC swap. In addition, note that, for the FX-TARN swap, although both uniform and non-uniform ADI methods used the same number of timesteps, only 30 gridpoints in the a-direction are employed for the non-uniform ADI method compared to 40 gridpoints for the uniform ADI method. Consequently, over each time period of the swap's tenor structure, the non-uniform ADI method must solve 30 PDEs (in parallel) whereas the uniform ADI method must solve 40 PDEs (in parallel). This results in a very significant reduction in the computational requirements for the non-uniform ADI method compared to the uniform ADI method.

We note that, to make a more rigorous efficiency comparison between the uniform and non-uniform ADI-FD methods, we should take into account the total cost of the ADI-FD methods. When utilizing the non-uniform ADI-FD method, certain additional costs arise, such as (i) interpolation at each date of the swap's tenor structure; (ii) matrix-vector multiplications in the Steps (3.5a) and (3.5c) of the ADI timestepping method (e.g. a nine-point (3×3) stencil for matrix-vector multiplications involving $\mathbf{A}_0^m$ on non-uniform grids versus a four-point one on uniform grids); and (iii) the timestep size selector. However, since these additional computational costs are only a small fraction of the method's total computational costs, it is still true that, for knockout and FX-TARN PRDC swaps, the non-uniform ADI-FD method is considerably more efficient than its uniform counterpart.

4.3.2. Analysis of pricing results

a) Effects of the leverage levels

We briefly review the prices of "vanilla" PRDC swaps, due to their relevance to our discussion later in the section. With the set of model parameters used in this paper, the computed prices for low-, medium- and high-leverage "vanilla" PRDC swaps are approximately -11.107%, -12.686% and -11.087%, respectively. (See [12, 14, 15]). (Note that, due to the impact of the FX volatility skew, the prices of "vanilla" PRDC swaps obtained under a FX skew model, such as the model used in this paper, are approximately the same for the low- and high-leverage cases, while are smaller, i.e. more negative, for the medium-leverage case. A detailed discussion in this regard can be found in the literature, e.g. in [34].) These results indicate that the investor who buys the “vanilla” PRDC swap should pay a net coupon of about 11.107%, 12.686% and 11.087%, respectively, of the notional to the issuer. Hence, from the perspective of the investor, “vanilla” PRDC swaps are not attractive, because the investor must pay the initial coupon.

On the other hand, for the knockout PRDC swaps considered above, for the low-, medium- and high-leverage cases under the FX skew model, the issuer should pay a net coupon of about 1.365%, 2.115% and 5.523% of the notional to the investor (see Table 4.4). For the low-leverage FX-TARN PRDC swap considered above, the investor should pay a net coupon of about 4.384% of the notional to the issuer. (Note the negative values in this case.) However, for the medium- and high-leverage cases, the issuer should pay the investor a net coupon of about 3.793% and 18.637%, respectively, of the notional. (See Table 4.5, non-uniform ADI-FD.) Compared to the “vanilla” PRDC swap, it is clear that, from the perspective of the investor, the knockout and FX-TARN features result in more positive prices for the swap. This is consistent with the discussion in Subsection 2.4. Of course, in all cases, the issuer would prefer to pay less, if the prices are positive, or to receive more, if the prices are negative, and keep the difference as profit.

Another observation is that, for both knockout and FX-TARN PRDC swaps, among the three leverage cases, the high-leverage case is the most attractive to the investor, due to the high initial coupon paid by the issuer to the investor. On the other hand, the low-leverage case is the least attractive to the investor, due to a smaller initial coupon, which may even be negative in some cases, resulting in an initial fund outflow for the investor. For example, for the low-leverage FX-TARN swap with $a_c = 50\%$, the investor must pay the initial coupon (although it is smaller than the coupon the investor must pay in the low-leverage case for a “vanilla” PRDC swap). This observation is consistent with the remarks in [34] for Bermudan cancelable PRDC swaps.

leverage level	a_c			
	10%	20%	50%	80%
low	5.367	1.231	-4.388	-6.847
medium	8.801	3.787	-3.133	-6.329
high	18.637	14.910	9.018	5.948

Figure 4.3: Prices of FX-TARN PRDC swaps for various target cap levels, a_c, and various leverage levels for the FX skew model using the finest mesh in Table 4.5 and the non-uniform ADI-FD method.

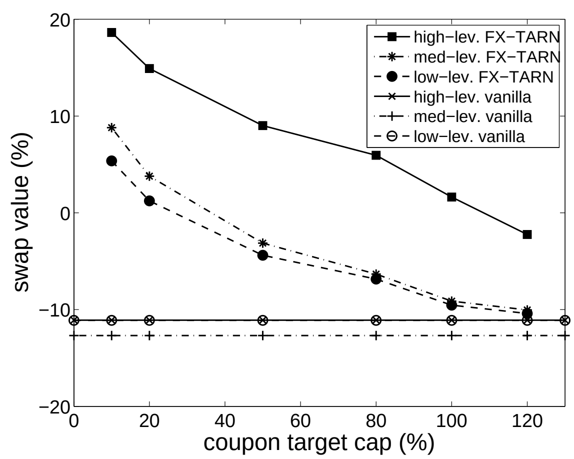

Figure 4.4: For large values of a_c, prices of FX-TARN PRDC swaps tend to the prices of “vanilla” PRDC swaps.

b) Effects of the target cap a_c

In Figure 4.3, we present selected prices for FX-TARN PRDC swaps for various values of the target caps a_c obtained using the finest mesh in Table 4.5, non-uniform ADI-FD. We observe that the price of a FX-TARN PRDC swap is a decreasing function of the target cap a_c. More specifically, a smaller value of the target cap a_c results in a more positive price of the FX-TARN PRDC swap, indicating that the issuer pays the investor the initial coupon (e.g. see the low-leverage case with $a_c = \{10\%, 20\%\}$). On the other hand, if the target cap a_c is large enough, the price could become negative, i.e. the investor pays the issuer the initial coupon (e.g. see the low-leverage case with $a_c = \{50\%, 80\%\}$). This behavior of the price of a FX-TARN PRDC swap is expected, since, the smaller the target cap is, the higher the leverage of the swap (from the perspective of the investor). On the other hand, the larger the value of the target cap is, the later the underlying PRDC swap is expected to terminate. As a result, a FX-TARN PRDC swap with a large target cap, a_c, tends to behave like a “vanilla” PRDC swap. Hence, the price of a FX-TARN PRDC swap with a large target cap, a_c, is close to the price of the “vanilla” swap, as shown in Figure 4.4.

c) Profiles of the swap values

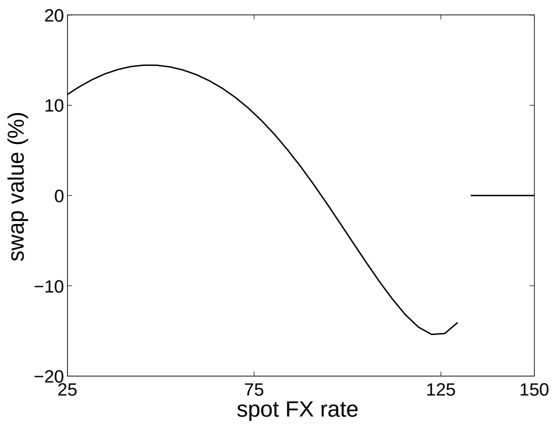

Figure 4.5: Values of knockout PRDC swaps, in percentage of N_d, as a function of the spot FX rate at time $T_{\alpha^+} \equiv T_{3^+} = 3$ with high-leverage coupons. The constant barrier is 131.25.

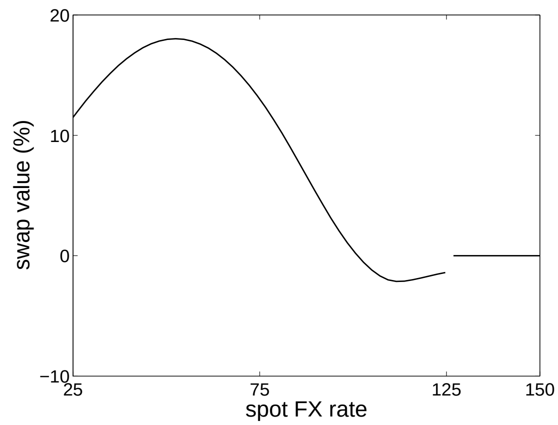

Figure 4.6: Values of FX-TARN PRDC swaps, in percentage of N_d, as a function of the spot FX rate at time $T_{\alpha^+} \equiv T_{3^+} = 3$ with high-leverage coupons and $a_{2^+} \equiv a_{3^-} \approx 6.25\%$. The computed barrier is 126.3.

To better understand the dynamics of knockout and FX-TARN PRDC swaps, we investigate the value of the knockout/FX-TARN swap at an intermediate date of the tenor structure as a function of the spot FX rate on that date. In Figure 4.5, we plot the value function for high-leverage knockout PRDC swaps immediately *after* the exchange of fund flows scheduled at time $T_\alpha = 3$, i.e. at time T_{3^+}, as a function of the spot FX rate on that date. Note that, this is a plot of the quantity $\hat{u}_{\alpha-1}(T_{\alpha^+})$ defined in (2.14) as a function of $s(T_\alpha)$, where $\alpha = 3$. Similarly, in Figure 4.6, we plot the value function for high-leverage FX-TARN PRDC swaps immediately *after* the exchange of fund flows scheduled at time $T_3 = 3$, given the accumulated PRDC coupon amount $a_{2^+} \equiv a_{3^-} < a_c$. This is essentially the plot of the quantity $u_{\alpha-1}(T_{\alpha^+}; a_{(\alpha-1)^+})$ defined in (3.14) as a function of $s(T_\alpha)$, for $\alpha = 3$. For the FX-TARN swap example considered in Figure 4.6, we let $a_{3^-} \approx 6.25\%$, whence, from (3.12), the computed knockout barrier is about 126.3. Note that, the strike k_α and the forward FX rate $F(0, T_\alpha)$ when $\alpha = 3$ are about 86.4 and 95.4, respectively.

For both the knockout and FX-TARN PRDC swaps, we observe that, in the region to the left of the strike, the value function is positive and concave-down, i.e. it has negative gamma. This agrees with the interpretations that (i) the swap is not pre-maturely terminated, due to low spot FX rates, and that (ii) the issuer has a short position in low-strike FX call option. (Recall that the issuer pays PRDC coupons, the rates of which can be viewed as call options on the spot FX rate, as indicated by the coupon rate formula (2.7). For the low-, medium-, and high-leverage cases, the strike $k_\alpha = \frac{c_d}{c_f} f_\alpha$ is set to 50%, 70% and 90% of

$f_\alpha \equiv F(0, T_\alpha)$, respectively, hence is significantly less than $s(0)$. As a result, the PRDC coupon rates defined by (2.7) can be viewed as low-strike FX call options.)

However, in the region to the right of the strike and tending to the barrier, as evident from Figures 4.5 and 4.6, the value function becomes negative and its profile changes from being concave-down to being concave-up, i.e. it has positive gamma. The value function becomes negative in this region because the higher PRDC coupon rates amount to fund outflows from the issuer's perspective. The change of concavity can be understood by noting that the underlying PRDC swap is canceled when $s(T_\alpha) \geq b$ (for the knockout swap) or $s(T_\alpha) \geq b_\alpha^y$ (for the FX-TARN swap). This can be interpreted as the issuer having a long position in high-strike FX call options. Hence, the profile of the value function changes from concave-down to concave-up to reflect this change from a short position in low-strike FX call options to a long position in high-strike FX call options.

The discussion above explains why the profile of a knockout or FX-TARN PRDC swap is similar to that of a bear spread created by call options[7], which is known to be very sensitive to the skewness of the FX volatility smile. These observations for knockout and FX-TARN PRDC swaps are similar to those reported in [34] for Bermudan cancelable PRDC swaps. However, a knockout/FX-TARN PRDC swap exhibits even more sensitivity to the FX volatility skew in the concave-up part, near the barrier, due to the discontinuity in the payoff function at the barrier. As a result, the overall impact of the FX volatility skew on the price of a knockout/FX-TARN PRDC swap is expected to be quite substantial. Since it is not a focus of this paper to discuss the impact of the FX volatility skew on the price of a knockout/FX-TARN PRDC swap, we limit our discussion of this important topic to a few brief remarks. Our experiments, reported in [12], indicate that, the three-factor FX skew model considered in this paper results in significantly lower prices (i.e. higher profits) of the knockout/FX-TARN swap for the issuer than those obtained under a similar three-factor log-normal model calibrated to the same market data.[8] Hence, from the perspective of the issuer, it is important to have a model that can accurately capture the skew of the FX volatility.

5. Conclusions and future work

We discussed efficient PDE-based methods to price foreign exchange interest rate hybrid derivatives, with particular emphasis on PRDC swaps with knockout and FX-TARN features, under a three-factor multi-currency pricing model with FX volatility skew. Due to the path-dependency of FX-TARN PRDC swaps, forward pricing algorithms, such as MC simulation, are the natural choice for pricing these derivatives. By introducing an auxiliary state variable to keep track of the total accumulated PRDC coupon to date, which stays constant between dates of the tenor structure and is updated on each date of the tenor structure by a PRDC coupon amount known on that date, we developed a PDE-based pricing algorithm for FX-TARN PRDC swaps which steps backward in time. This approach requires us to solve a set of independent model PDEs for each of the discretized values of the auxiliary state variable over each period of the swap's tenor structure, with communication at the end of the period only. We showed that each of these pricing sub-problems can be viewed as equivalent to a knockout PRDC swap with a time-dependent step-down barrier, the solution of which can be computed by solving a time-dependent parabolic PDE in three space dimensions. We investigated the construction of certain pre-determined non-uniform grids for use with second-order cen-

[7] A bear spread can be created using call options by going short a low-strike call option and going long a higher-strike call option with the same maturity.

[8] Here, a log-normal model refers to a model in which the local volatility function is a deterministic function of the time variable t only, and does not depend on the spot FX rate s.

tered FD discretizations for the space variables of the model PDE, while utilizing efficient timestepping ADI techniques, combined with a simple, but effective, timestep size selector, for the time discretization of the PDE. Our numerical results confirm the validity of the PDE pricing approach and the convergence properties of numerical methods. They also show that suitably constructed non-uniform computational grids can substantially improve the efficiency of numerical methods for pricing cross-currency/FX interest rate derivatives, especially swaps with knockout/FX-TARN features.

We conclude by mentioning some possible extensions of this work. It would be desirable to have a theoretical analysis of the second-order convergence of the ADI timestepping method on non-uniform grids for three-dimensional time-dependent parabolic PDEs. From a numerical methods perspective, it would be interesting to investigate the effects of higher-order interpolation schemes, such as cubic splines, on the swaps' prices. To further increase the efficiency of the numerical methods, higher-order spatial and time discretization methods can be employed. For example, the fourth-order (optimal) quadratic spline collocation (QSC) method developed in [5], which requires the solution of only one tridiagonal linear system at each timestep, could be utilized in combination with a fourth-order ADI time-stepping method. To achieve even a higher efficiency, adaptive techniques, such as those developed in [6, 30], which dynamically adjust the location of the gridpoints to control the error in the approximate solution, could be used.

Several extensions to the model adopted in this paper could be studied. Firstly, due to the sensitivity of PRDC swaps with exotic features to the FX volatility skew, it would be desirable to have a model that more accurately approximates the observed FX volatility skew. In this regard, one approach is to model the variance of the spot FX rate using a stochastic process, such as the Heston model [23], so that the market-observed FX volatility smiles are more precisely captured. Another possible direction worth investigating is to retain the standard three-factor model, and instead of having a local volatility function, use a regime switching model [3, 18] for the stochastic volatility of the spot FX rate. Secondly, since one-factor interest rate models cannot provide realistic evolutions of the term structures over a very long time period, such as the typical maturity of a PRDC swap, multi-factor Gaussian interest rate models, such as two- or three-factor Hull-White models, should be explored.

As an enriched model may have significantly more than three stochastic factors, a PDE-based pricing approach becomes less suitable, due to the "curse of dimensionality" associated with high-dimensional PDEs. While a MC pricing approach is the popular choice in this case, the main challenge is to find an effective variance reduction technique. To this end, a hybrid pricing method, combining the MC and PDE approaches, might be attractive. More specifically, one could possibly use a highly accurate numerical solution obtained from the standard model with a local volatility function via the PDE approach developed in this paper as a control variate to accelerate the convergence of numerical solutions obtained from an enriched model using MC simulations.

References

[1] L. B. Andersen and V. V. Piterbarg, *Interest Rate Modeling*, Atlantic Financial Press, first ed., 2010.

[2] C. Beveridge, M. Joshi, and W. Wright, *Efficient pricing and Greeks in the cross-currency LIBOR market model*, SSRN eLibrary, (2010). Available at http://ssrn.com/abstract=1662229.

[3] N. Bollen, S. F. Gray, and R. E. Whaley, *Regime switching in foreign exchange rates: Evidence from currency option prices*, Journal of Econometrics, 94 (2000), pp. 239–276.

[4] D. Brigo and F. Mercurio, *Interest Rate Models - Theory and Practice*, Springer, second ed., 2006.

[5] C. Christara, T. Chen, and D. M. Dang, *Quadratic spline collocation for one-dimensional linear parabolic partial diffential equations*, Numerical Algorithms, 53 (2010), pp. 511–553. doi:10.1007/s11075-009-9317-9, http://www.springerlink.com/content/v1g8565702373446/.

[6] C. Christara and D. M. Dang, *Adaptive and high-order methods for valuing American options*, Journal of Computational Finance, 14 (2011), pp. 73–113.

[7] C. C. Chu and Y. K. Kwok, *Target redemption notes*, Journal of Futures Markets, 27 (2007), pp. 535–554.

[8] J. Cox, J. Ingersoll, and S. Ross, *An intertemporal general equilibrium model of asset prices*, Econometrica, 53 (1985), pp. 363–384.

[9] ——, *A theory of the term structure of interest rates*, Econometrica, 53 (1985), pp. 385–407.

[10] J. Crank and P. Nicolson, *A practical method for numerical evaluation of solutions of partial differential equations of the heat-conduction type*, Mathematical Proceedings of the Cambridge Philosophical Society, 43 (1947), pp. 50–67.

[11] D. M. Dang, *Pricing of cross-currency interest rate derivatives on Graphics Processing Units*, in Proceedings of the International Symposium on Parallel & Distributed Processing (IPDPS), IEEE Computer Society, 2010, pp. 1–8.

[12] ——, *Modeling multi-factor financial derivatives by a Partial Differential Equation approach with efficient implementation on Graphics Processing Units*, PhD thesis, Department of Computer Science, University of Toronto, Toronto, Ontario, Canada, 2011.

[13] D. M. Dang, C. Christara, and K. Jackson, *A parallel implementation on GPUs of ADI finite difference methods for parabolic PDEs with applications in finance*, Canadian Applied Mathematics Quarterly (CAMQ), 17 (2009), pp. 627–660.

[14] ——, *GPU pricing of exotic cross-currency interest rate derivatives with a foreign exchange volatility skew model*, To appear in the Journal of Concurrency and Computation: Practice and Experience, (2013). http://onlinelibrary.wiley.com/doi/10.1002/cpe.2824/abstract.

[15] D. M. Dang, C. C. Christara, K. Jackson, and A. Lakhany, *A PDE pricing framework for cross-currency interest rate derivatives*, in Proceedings of the 10th International Conference In Computational Science (ICCS), vol. 1, Procedia Computer Sciences, Elsevier, 2010, pp. 2371–2380.

[16] M. Dempster and J. Hutton, *Numerical valuation of cross-currency swaps and swaptions*, Cambridge University Press, 1997.

[17] J. Douglas and H. Rachford, *On the numerical solution of heat conduction problems in two and three space variables*, Trans. Amer. Math. Soc, 82 (1956), pp. 421–439.

[18] J. Duan, I. Popova, and P. Ritchken, *Option pricing under regime switching*, Quantitative Finance, 2 (2002), pp. 116–132.

[19] P. A. FORSYTH AND K. VETZAL, *Quadratic convergence for valuing American options using a penalty method*, SIAM J. Sci. Comput., 23 (2002), pp. 2095–2122.

[20] W. GROPP, E. LUSK, AND A. SKJELLUM, *Using MPI-2: Advanced Features of the Message Passing Interface*, MIT Press, first ed., 1999.

[21] ——, *Using MPI: portable parallel programming with the message-passing interface*, MIT Press, second ed., 1999.

[22] T. HAENTJENS AND K. J. IN 'T HOUT, *Alternating direction implicit finite difference schemes for the Heston-Hull-White partial differential equation*, Journal of Computational Finance, 16 (2012), pp. 83–110.

[23] S. L. HESTON, *A closed-form solution for options with stochastic volatility with applications to bond and currency options*, Review of Financial Studies, 6 (1993), pp. 327–343.

[24] J. HULL AND A. WHITE, *One factor interest rate models and the valuation of interest rate derivative securities*, Journal of Financial and Quantitative Analysis, 28 (1993), pp. 235–254.

[25] W. HUNDSDORFER, *Accuracy and stability of splitting with stabilizing corrections*, Appl. Numer. Math, 42 (2002), pp. 213–233.

[26] W. HUNDSDORFER AND J. VERWER, *Numerical Solution of Time-Dependent Advection-Diffusion-Reaction Equations*, *Springer Series in Computational Mathematics*, vol. 33, Springer-Verlag, Berlin, 2003.

[27] K. J. IN 'T HOUT AND B. D. WELFERT, *Stability of ADI schemes applied to convection-diffusion equations with mixed derivative terms*, Appl. Numer. Math. 57 (2007), pp. 19–35.

[28] ——, *Unconditional stability of second-order ADI schemes applied to multi-dimensional diffusion equations with mixed derivative terms*, Appl. Numer. Math. 59 (2009), pp. 677–692.

[29] C. JEFFERY, *The problem with Power-Reverse Duals*, Risk magazine, 16 (2003), pp. 20–22.

[30] P. LÖTSTEDT, J. PERSSON, L. V. SYDOW, AND J. TYSK, *Space-time adaptive finite difference method for European multi-asset options*, Computers & Mathematics with Applications, 53 (2007), pp. 1159–1180.

[31] M. MELVIN AND M. P. TAYLOR, *The crisis in the foreign exchange market*, Journal of International Money and Finance, 29 (2009), pp. 1317–1330.

[32] A. MIJATOVIC AND M. PISTORIUS, *Continuously monitored barrier options under Markov processes*, Mathematical Finance, 23 (2013), pp. 1–38.

[33] M. MUSIELA AND M. RUTKOWSKI, *Martingale methods in financial modelling*, Springer, second ed., 2005.

[34] V. PITERBARG, *Smiling hybrids*, Risk magazine, 19 (2006), pp. 66–70.

[35] V. V. Piterbarg, *TARNs: Models, Valuation, Risk Sensitivities*, Wilmott magazine, 14 (2004), pp. 62–71.

[36] D. M. Pooley, K. R. Verzal, and P. A. Forsyth, *Convergence remedies for non-smooth payoffs in option pricing*, Journal of Computational Finance, 6 (2003), pp. 25–40.

[37] R. Rannacher, *Finite element solution of diffusion problems with irregular data*, Numerische Mathematik, 43 (1984), pp. 309–327.

[38] J. Sippel and S. Ohkoshi, *All power to PRDC notes*, Risk magazine, 15 (2002), pp. 1–3.

[39] C. C. Tan, *Demystifying exotic products*, John Wiley & Sons, Inc., 2010.

[40] D. Tavella and C. Randall, *Pricing financial instruments: The finite difference method*, John Wiley & Sons, Chichester, 2000.

[41] B. A. Wade, A. Q. M. Khaliq, M. Yousuf, J. Vigo-Aguiard, and R. Deiningere, *On smoothing of the Crank-Nicolson scheme and higher order schemes for pricing barrier options*, Journal of Computational and Applied Mathematics, 204 (2007), pp. 144–158.

[42] H. Windcliff, P. A. Forsyth, and K. R. Vetzal, *Analysis of the stability of the linear boundary condition for the Black-Scholes equation*, Journal of Computational Finance, 8 (2004), pp. 65–92.

[43] R. Zvan, P. Forsyth, and K. Vetzal, *Discrete Asian barrier options*, Journal of Computational Finance, 3 (1999), pp. 41–68.